AD NUMBER

AD451245

NEW LIMITATION CHANGE

TO

Approved for public release, distribution unlimited

FROM

Distribution authorized to U.S. Gov't. agencies and their contractors; Administrative/Operational Use; OCT 1964. Other requests shall be referred to Army Research Office, Triangle Park, NC.

AUTHORITY

US ARO Ctr ltr, 27 May 1966

INDIANA UNIVERSITY
CHEMICAL LABORATORY

UNITED STATES OFFICE OF ARMY RESEARCH
O.A.R. CONTRACT DA-33-008-ORD-1989
1 July 1960 - 15 August 1963

APPLICATIONS OF IONIC BEAMS TO STUDY OF CORROSION OF METALS BY GASES

PRINCIPAL INVESTIGATOR: WALTER J. MOORE

OCTOBER 1964

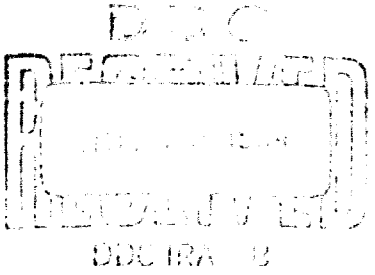

Bloomington, Indiana

FINAL REPORT

APPLICATION OF IONIC BEAMS TO STUDY OF CORROSION OF METALS BY GASES

October 1964

OOR PROJECT NO. 2692 C

O.A.R. CONTRACT NO. DA-33-008-ORD-1989

PRINCIPAL INVESTIGATOR: WALTER J. MOORE

AUTHORS: Walter J. Moore, Sigemaro Nagakura, Nguyen Trinh Dzoanh, Derek Klemperer, and Jens Traetteberg

TABLE OF CONTENTS

APPLICATIONS OF IONIC BEAMS TO STUDY OF GASEOUS CORROSION OF METALS

Principal Investigator . Walter J. Moore

INTRODUCTION

The final report of our work on this contract is given in the form of a collection of preprints of papers based on various sections of the work.

This research program was conducted under unusually difficult conditions. The kind of exploratory research that we wanted to do was not at all suited for students working toward their first research degrees. Thus we decided to rely mainly on postdoctoral research associates and research technicians. As it turned out, for various good reasons, only one of the three research associates could stay with us more than one year, and the appointment of the last one had to be terminated when our funds were exhausted. We thus lost considerable time as continuity of the work was interrupted. Another difficulty was the lack of funds to buy commercially made equipment, such as high vacuum valves and pumps. We thus used a fair part of our time in construction of equipment. My final conclusion is that this kind of exploratory research is more expensive than the usual university research. To obtain good results quickly, one should be able to buy the necessary equipment and thus begin the active experiments sooner. One also needs at least some permanent staff in addition to the principal investigator.

Nevertheless, with all the difficulties we accomplished more or less what we stated we would do in the contract application. In most cases,

TABLE OF CONTENTS

however, the work was not really brought to a definite finishing point -- interesting experiments were made, preliminary results were obtained, but definitive results and conclusions were not achieved. To this extent, the program has raised more interesting problems than it has solved. Perhaps other workers interested in gaseous corrosion will find in this work an indication of useful new directions to explore.

We should like to acknowledge the good work of our research technicians Sylvester Brown and Howard Brown, as well as valuable contributions by Earl Sexton, master glassblower, and Jack Baird, machinist.

The following research associates worked on the program. Present addresses are given.

Dr. Derek Klemperer, University of Bristol

Dr. Sigemaro Nagakura, Tokyo Institute of Technology

Dr. Nguyen Trinh Dzoanh, Illinois Institute of Technology

Dr. Jens Traetteberg, University of Trondheim

EFFECTS OF ATOMIC OXYGEN ON SEMICONDUCTOR OXIDES

NGUYEN TRINH DZOANH and WALTER J. MOORE

Chemical Laboratory, Indiana University, Bloomington

The behavior of inorganic solids in an atmosphere containing a controlled concentration of atoms and other labile species has never been studied systematically, as far as semiconductor properties are concerned. Some works however, are devoted exclusively to the study of surface catalytic properties of these crystals for atom recombination.[1-4]

The presence of oxygen atoms would increase the chemical potential of the oxygen in contact with a semiconductor oxide and promote the mechanism of cationic vacancy diffusion in the solid oxide. Among the oxides which might behave in this manner when in contact with an oxygen-atom atmosphere, we shall direct our attention first to the case of nickel oxide and generalize to the others later.

CONDUCTIVITY OF NICKEL OXIDE

According to Verwey, et al.,[5] the conductivity of NiO results from the excess positive charges due to Ni^{3+} ions on normally Ni^{2+} lattice sites. When given a sufficient amount of energy, these positive holes may be transferred from the Ni^{3+} ions to the Ni^{2+} ions. The charge spends a finite length of time at each site, as in a diffusion process, and under an electrical potential gradient, the charges may be transferred. In such a model the conductivity should be proportional to the concentration of the Ni^{3+} ions. This concentration in the bulk may be increased or decreased by the incorporation of foreign ions of lower or higher valency than two, as is clearly shown by the work of Hauffe, et al.,[6] and recently by VanHouten.[7] An increase in the

Ni^{3+} concentration without doping is based on the characteristic departure of the NiO from exact stoichiometry in the direction of excess oxygen.

Deviation from Stoichiometry

Engell and Hauffe[8] concluded from their kinetic analysis that when NiO is exposed to an oxygen atmosphere, two processes occur: chemisorption and structural incorporation. The adsorption of oxygen involves the formation of stable oxide ions and cation vacancies. At high enough temperatures, adsorbed oxygen is incorporated into the surface layer of the NiO structure by outward diffusion of Ni^{2+} ions. This diffusion generates further sites for oxygen uptake[9] and provides a mechanism for a continuing slow adsorption. However, recent evidence[10] suggests that the excess oxygen is located only near the surface, even at high temperatures. Excess oxygen in NiO is then accommodated by the reaction,

$$(1)\quad \tfrac{1}{2}O_2 \rightarrow O^{2-} + V_{(Ni^{2+})} + 2p$$

where $V_{(Ni^{2+})}$ indicates vacant sites and p, positive holes.

The vacancies provide a mechanism for diffusion of metal ions[11] in the crystal and the associated positive holes are expected to be localized on Ni^{3+} ions, resulting in an increase in conductivity. When thermodynamic equilibrium is established with the surrounding atmosphere, the concentration of Ni^{3+} ions will change according to the reversible equation,

$$(2)\quad \tfrac{1}{2}O_2 + 2Ni^{2+} \rightleftarrows O^{2-} + 2Ni^{3+} + V_{(Ni^{2+})}\ .$$

Using the ideal mass action law, the equilibrium constant is obtained:

$$(3)\quad K = \frac{\left[Ni^{3+}\right]^2 \left[V_{(Ni^{2+})}\right]}{(P_{O_2})^{\frac{1}{2}}}$$

The activities of Ni^{2+} and O^{2-} are taken as unity because deviation from stoichiometric NiO is slight. If other disorder equilibria are negligible, since there are two Ni^{3+} ions for each vacancy, charge neutrality requires

$$(4) \quad \left[Ni^{3+}\right] = 2\, V_{(Ni^{2+})} .$$

Equation (3) will be

$$K = \left[Ni^{3+}\right]^3 / 2(P_{O_2})^{\frac{1}{2}}$$

$$(5) \quad \left[Ni^{3+}\right] = (2K)^{1/3}(P_{O_2})^{1/6}$$

$$= (2)^{1/3}(P_{O_2})^{1/6} \exp\,(-\Delta G_f^\circ/3RT) .$$

$\Delta G_f^\circ = \Delta H_f^\circ - T\Delta S_f^\circ$ indicates the free energy of defect formation for the reaction of equation (2). If the conductivity is, as shown above, proportional to $\left[Ni^{3+}\right]$, then

$$(6) \quad \sigma = \left[Ni^{3+}\right] q\mu,$$

where q and μ indicate charge and mobility of the positive holes. On substituting $\left[Ni^{3+}\right]$ in (6), we have

$$(7) \quad \sigma = q\mu(2)^{1/3}(P_{O_2})^{1/6} \exp\,(-\Delta G_f^\circ/3RT)$$

$$= A(P_{O_2})^{1/6} \exp\,(-\Delta G_f^\circ/3RT)$$

where $A = q\mu(2)^{1/3}$. We see from (4), (5), and (7) that the departure from stoichiometry by formation of positive holes depends on the ambient oxygen pressure at a given temperature.

Clearly the concentration of cation vacancies and the associated positive holes can be varied over a certain range by variation of the temperature and the oxygen pressure. Many such studies have been made of nonstoichiometric

oxides, but the extent of the range has been found to be often severely limited, except perhaps at extremely high pressures. We thought that a convenient and interesting way to raise the chemical potential of the oxygen in contact with the oxide crystal would be to expose the crystal to an ambient atmosphere containing a concentration of oxygen atoms.

When in contact with the semiconductor oxide, some oxygen atoms will be lost by surface recombination due to the catalytic properties of the NiO crystal.[3] If the oxygen atom loss is not too high, a steady state should be reached, with an increase of the number of positive holes and therefore the conductivity of the crystal. We can then follow the process by exposing to the gas stream a thin slice of NiO mounted with electrodes for conductivity measurements.

EXPERIMENTAL DETAILS

The experim ntal arrangement is shown in Fig. 1. The oxygen atoms were produced by a rf discharge in a fast flow system. The pumping system was a conventional one, consisting of a high speed single stage mercury diffusion pump backed by a rotary pump. The discharge was maintained with a high frequency communication transmitter tube type 829-B, operating at a frequency of 60 Mc/s. Its power rating was 70 watts, but in practice the maximum power used was slightly lower. The discharge always had a tendency to spread into the measuring zone. In order to avoid this inconvenience, Jennings and Linnett[12] suggested an earthed metal screen placed between the discharge tube and the coil, but in our system the result was not satisfactory. Finally we applied a strong magnetic field at about 2 cm down stream from one end of the coil, and a small earthed metal ring around the discharge tube was used to minimize the influence of the high frequency electric field in this area. The result

[illegible]. It was possible in this way to localize the discharge zone and all charged particles which might have been able to create undesirable spreading discharges could not approach this "forbidden area" because of the strong power of reflection of the magnetic force.

The discharge tube of Pyrex and the 2.5 cm outer diameter reaction tube of quartz or silica (for heating purposes) were often cleaned with dilute hydrofluoric acid and repeated rinsing in distilled water. Tank oxygen, supplied by the Matheson Company, was used without purification. The impurities in oxygen primarily H_2 and H_2O should have a catalytic effect for oxygen atom production.[13] The flow rate was adjusted by means of fine control needle valves and measured by calibrated capillary flowmeters. The pressure in the main tube was measured by a thermocouple gauge and a Penning ionization gauge. The concentration of oxygen atoms was measured 35 cm down stream from the discharge zone by means of an isothermal calorimetric detector. This device was first developed for the hydrogen-atom reaction studied by Tollefson and Leroy[14] and modified later by other investigators.[4] It consists of a spiral platinum wire coated with silver by electroplating. When submitted to an atmosphere containing oxygen atoms the silver is rapidly converted to the oxide which forms an excellent catalyst for oxygen atom recombination without further oxidation.

In order to minimize the error due to the heat loss (radiation, thermal conductivity, etc.) the compensation method was used to measure the heat released by recombination from which the oxygen-atom concentration could be deduced. The flow rate F of atomic species is given by

$$F = \frac{R(I_0^2 - I^2)}{4.18\,\Delta H}$$

where R is the resistance of the silver coated platinum wire at the chosen temperature. I_0 and I are the measured currents in the absence and presence

of oxygen atoms, and $\Delta H = 59.5$ kcal/mole is the heat of recombination per mole of atomic oxygen.

Resistance measurements were made on a single crystal of NiO supplied by the Tochigi Chemical Industry Company, Osaka, Japan. Spectrographic analysis showed that the crystal contained 0.6% cobalt and 0.1% magnesium, with traces of other elements. The crystal was cleaned and then polished flat on a precision grinder using silicon carbide paper of grades 1/0 to 4/0. The specimen of approximately 1.5 x 4 mm^2 and 0.1 mm thick was cleaned with dilute nitric acid and distilled water before use.

EXPERIMENTAL RESULTS AND DISCUSSION

A. Production of atomic oxygen. The first series of experiments was designed to establish the pressure dependence of the dissociation of O_2 and therefore, the flow rate of atomic oxygen, in order to determine the optimum working condition for further studies on the effect of oxygen atoms on nickel oxide. It is, of course, interesting to work at relatively high pressure, but unfortunately the ability of the rf electric field to maintain a discharge rather limits the experiment to low pressures. At higher pressure the electrons seem to be unable to gain sufficient energy between collisions. Microwave radiation would be more suitable to maintain a discharge at this upper range of pressure. In our experiments, the rf discharge became unstable and extinguished at a pressure above 0.5 torr. With oxygen at about 0.1 torr, the discharge was white, tinged with green. As the pressure increased it became red-mauve in color. The production of atomic oxygen versus the gas pressure at room temperature is shown in Figure 2, and the atomic oxygen pressure in Table I. The highest concentration of oxygen atoms is produced at a pressure of approximately 350 microns, but in order to avoid some inconvenience due to the instability of the discharge, it was decided to work at a slightly lower pressure.

TABLE I. (Temperature 298°K)
Oxygen Atom Concentrations in Flow System

Total pressure (torr)	O-Flow rate (mol sec^{-1} x 10^7)	O_2-Flow rate (mol sec^{-1} x 10^7)	$\frac{F_O}{F_{O_2}}$ x 10^2	Pressure O-atom x 10^2 (torr)
0.4	7.00	64	11.2	4.48
0.3	7.85	58.5	13.4	4.02
0.2	5.38	44.5	12.1	2.42
0.15	3.20	30	10.66	1.60
0.1	1.42	17.5	8.10	0.81
0.05	0.66	9.9	6.66	0.36

B. Presence of ozone and other species. Some ozone as well as some small amount of other metastable species is expected to be produced by the rf discharge by the reaction: $O + O_2 \longrightarrow O_3$, but at the low pressure, and high temperatures used in these experiments, the ozone must decompose so rapidly that its concentration in the gas stream, if any, should be extremely low and therefore negligible. This hypothesis is supported by a mass spectrometric study of oxygen at 0.5 mm Hg pressure subjected to an ac glow discharge.[15] Charged particles should not occur in the measuring section. Some tests were done to detect any which might have been attracted from the discharge zone, either by diffusion or under the influence of the dc potential applied to the target for conductivity measurements. It was shown that no charged particles existed in the measuring section.

C. Effect of oxygen atoms. At the chosen temperature and pressure, the NiO specimen was subjected to the gas stream containing atoms produced by a rf discharge during two hours. The behavior of its conductivity was followed by the change of its resistance during the rf discharge and also two hours after the rf discharge. The slight change of temperature during this operation was recorded in the same time. It is shown in Figure 3

[illegible] the [illegible] the sudden decrease of the resistance was [illegible] the recombination effect which raised the temperature of the [illegible] and the superimposed effect of cationic diffusion, which has been [illegible]. After ten minutes, the steady state was established and the resistance gradually decreased at constant temperature. This change was no doubt due to the diffusion of metal ions in the crystal which created [illegible] positive holes.

When the discharge was cut off and the surface recombination effect was over, the specimen cooled slowly back to the initial temperature, but the resistance R of the specimen did not come back to the initial value R_0.

The resistance difference, $\Delta R = R_0 - R$, is a consequence of the oxygen incorporation into the surface layer of the NiO structure by outward diffusion of Ni^{2+} ions during the experiment. The effect of oxygen atoms on the electrical behavior of the nickel oxide can be evaluated in terms of pressure change at constant temperature. The conductivity σ_{O_2} of NiO in the presence of molecular oxygen is proportional to $(P_{O_2})^{1/6}$ as shown in formula (7). When the oxygen atoms are generated and incorporated in the crystal, the conductivity of NiO increases from σ_{O_2} to $\sigma_{(O_2 + O)}$. The latter is proportional to the equivalent pressure $[P_{(O_2 + O)}]^{1/6}$. The ratio $\frac{\sigma_{(O_2 + O)}}{\sigma_{O_2}}$ at constant temperature, given in Figure 5, is equal to 3.06/2.47 = 1.235. We have then

$$\frac{\sigma_{(O_2 + O)}}{\sigma_{O_2}} \simeq \left[\frac{P_{(O_2 + O)}}{P_{O_2}}\right]^{1/6} = 1.235.$$

The equivalent pressure $P_{(O_2 + O)}$ in this experiment was found to be 3.55 times higher than the pressure of molecular oxygen P_{O_2} prior to the gas [illegible]:

$P_{(O_2 + O)} \simeq 3.55\ P_{O_2}$.

The resistance of the NiO specimen decreased linearly with the time. The coefficient of proportionality given by the curve (3) is 75/100. We have then

$$\frac{\Delta R}{\Delta t} = \frac{-75}{100} \text{ ohms sec}^{-1} .$$

The dimension of the specimen was about 1.5 x 4 x 0.1 mm. Thus the specific resistivity of the nickel oxide decreased regularly at about 4.5 ohm cm every second.

D. Influence of high temperature. The change of the nickel oxide conductivity when submitted to the oxygen atom atmosphere during a ten minute period was measured at constant pressure and at various temperatures. The results are recorded in Figure 4. The effect of oxygen on the conductivity of the nickel oxide was evident up to the temperature of about 750°C. Above that the results obtained were irregular and the effect seemed to be decreased. This result seemed to be in contradiction with what was expected, because at higher temperatures the cationic diffusion should be more rapid, and therefore, the effect of oxygen atoms in creating new defects in the crystal should be higher. These facts could only be attributed to a decrease of the oxygen atom concentration when the temperature increases. The surface recombination coefficient γ for oxygen atoms on NiO, as well as on the reaction tube of silica and other components at the reaction area, would increase considerably at high temperature. The exact value of the coefficient γ at high temperature is not known for the nickel oxide, but for silica, for example, Linnett and Greaves[16] have shown that γ increases by a factor of one hundred from 1.6×10^{-4} at 20°C to 1.4×10^{-2} at 600°C, following a parabolic law. The slope, $\Delta\gamma/\Delta T$ of the curve γ versus temperature is rather steep. The same effect was found for potassium chloride ($\gamma_{20°} = 0.5 \times 10^{-4}$, $\gamma_{400°} = 1.5 \times 10^{-2}$). It can, therefore, be deduced that at temperatures above 600°C the coefficient γ would be high. If we speculate that the variation of

γ with temperature for NiO follows the same law as that for silica or potassium chloride, it is possible to obtain an approximate value of the surface recombination γ of oxygen atom for NiO at 600°C. At 20°C, γ for NiO is 7.7×10^{-3}.[3] Thus at 600°C it would be about 8×10^{-1} or more. This means that almost every oxygen atom striking the nickel oxide surface would recombine; therefore, the only net result would be to raise the temperature of the specimen.

These considerations appear to explain the small effect of oxygen atoms on the conductivity of NiO when the temperature is too high, as is shown in Figure 4.

E. Measurement of oxidation rate in atomic-oxygen atmosphere. In order to clarify this problem, the oxidation rate of copper was measured in atomic-oxygen and molecular-oxygen atmospheres. Thin foils of pure copper of about 1 cm^2 were oxidized at a temperature of 850°C and a pressure of 0.3 torr in both cases. These specimens were cleaned in a dilute solution of nitric acid, rinsed with distilled water, and dried in nitrogen prior to oxidation. They were carefully weighed on a microbalance before and after the oxidation. The mass of oxygen uptake versus the square root of time is reported in Figure 5. The oxidation rate in an oxygen-atom atmosphere still follows the parabolic law, but is higher $[(\Delta m)_{t,O} > (\Delta m)_{t,O_2}]$ and faster than that in molecular oxygen:

$$\left[\frac{\Delta m}{\sqrt{t}}\right]_{\text{atoms}} > \left[\frac{\Delta m}{\sqrt{t}}\right]_{\text{molecules}}.$$

This difference might be explained by the fact that the surface recombination coefficient γ of oxygen atoms in contact with metal is nearly equal to unity. As soon as a thin oxide film was formed, the coefficient γ became lower and the effect of oxygen atoms was accentuated. However, the effect of an atomic-oxygen atmosphere on the oxidation of metal was not great. Thus it appears that at high temperature most of the oxygen atoms in the gas stream recombine

[illegible] in contact with the hot oxidizing metal. The effects of atomic oxygen on the properties of cuprous oxide are thus small, as in the case of the nickel oxide previously discussed.

Although we cannot generalize on the basis of these two instances, the present work suggests that many metals that have protective oxide coatings will withstand oxidation by atomic oxygen at elevated temperatures nearly as well as they withstand oxidation by molecular oxygen.

REFERENCES

1. V. V. Voevodskii and G. K. Lavrovskaya, Dokl. Akad. Nauk. SSSR 63, 351 (1948).
2. G. K. Lavrovskaya and V. V. Voevodskii, Zh. Fiz. Khim. 25, 1050 (1951).
3. J. W. Linnett and D. G. H. Marsden, Proc. Roy. Soc. A 234, 489, 504 (1956).
4. J. C. Greaves and J. W. Linnett, Trans. Faraday Soc. 54, 1323 (1958).
5. E. J. W. Verwey, et al., Philips Research Reports 5, 173 (1950).
6. K. Hauffe and A. L. Vierk, Z. Physik. Chem. 196, 160 (1950).
7. S. Van Houten, J. Phys. Chem. Solids 17, 7 (1960).
8. H. J. Engell and K. Hauffe, Z. Elektrochem. 57, 762, 773 (1953).
9. R. M. Dell and F. S. Stone, Trans. Faraday Soc. 50, 501 (1954).
10. H. Gossel, Z. Elektrochem. 65, 98 (1961).
11. C. E. Birchenall. Met. Rev. 3, 235 (1958).
12. K. R. Jennings and J. W. Linnett, Nature 182, 597 (1958).
13. F. Kaufman and J. R. Kelso, J. Chem. Phys. 32, 301 (1960).
14. E. L. Tollefson and D. J. Le Roy. J. Chem. Phys. 16, 1057 (1948).
15. H. I. Schiff. Annals of New York Acad. Sci. 67, 518 (1957).
16. J. C. Greaves and J. W. Linnett Trans. Faraday Soc. 55 1351 (1959).

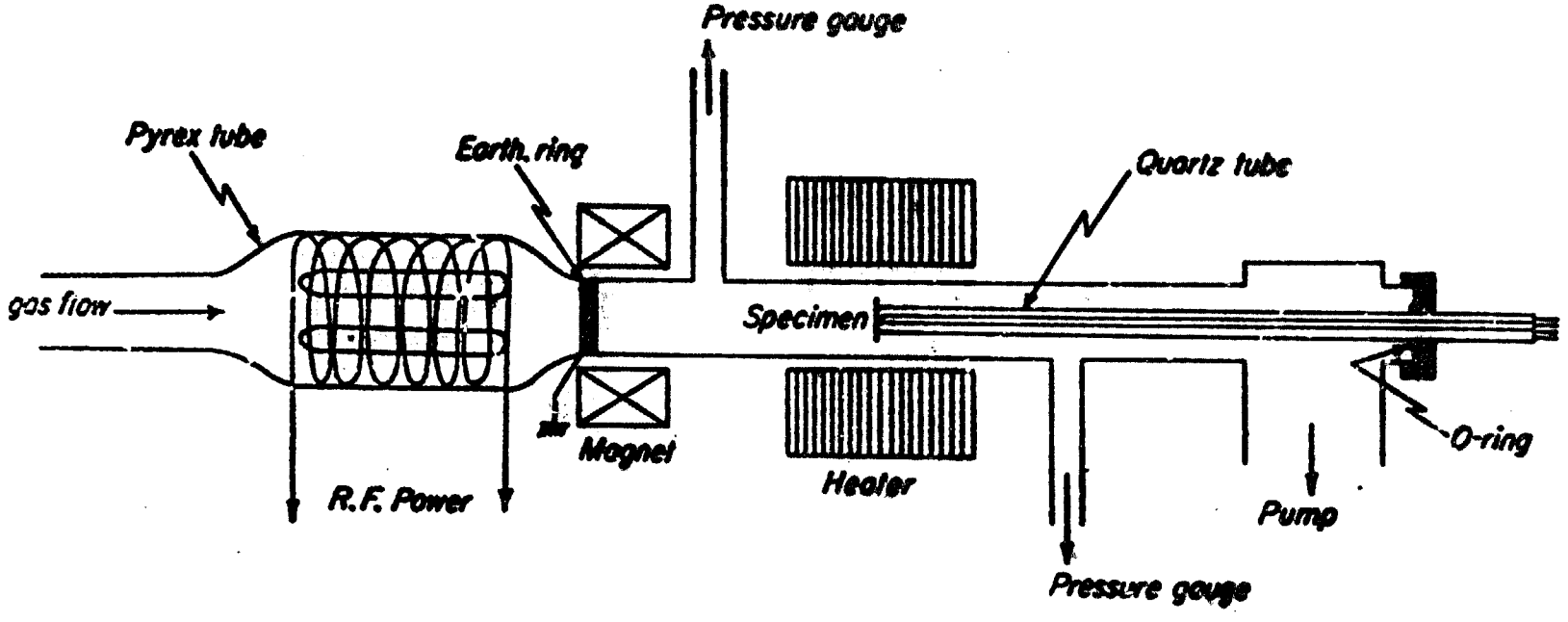

Fig. 1. Experimental arrangement for measuring conductivity of oxide crystal exposed to oxygen atoms.

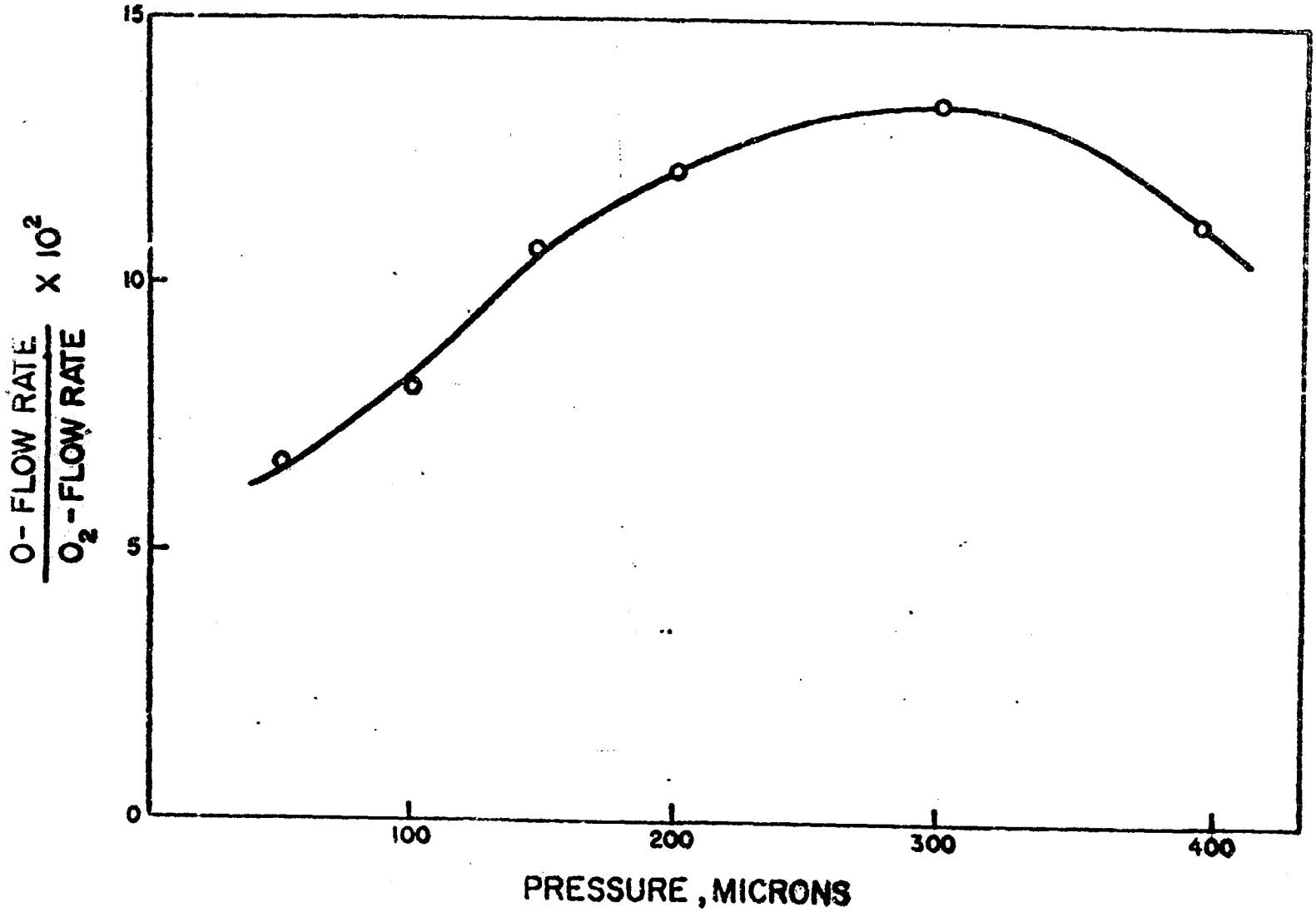

Fig. 2. Atomic oxygen concentration in flowing gas as a function of pressure.

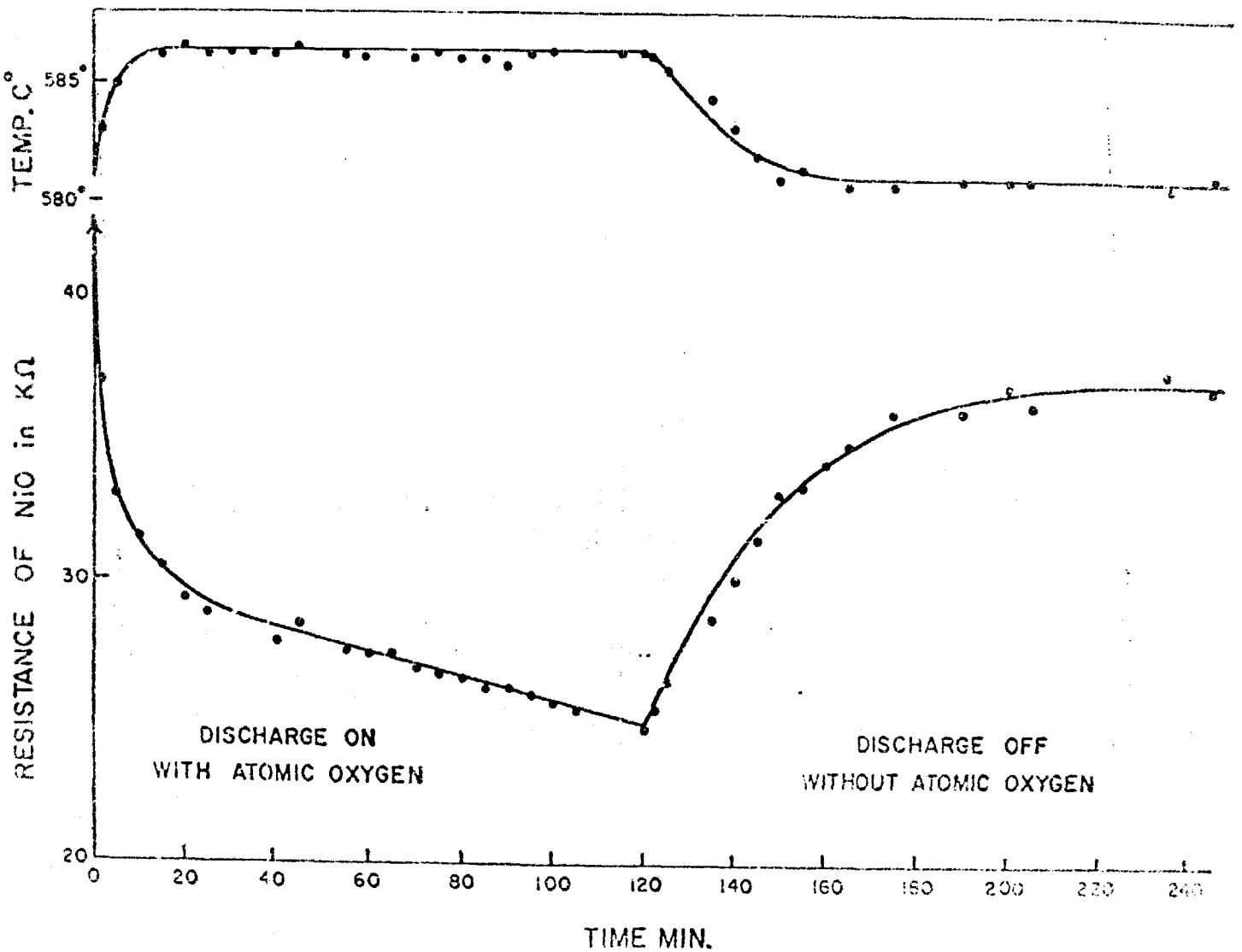

Fig. 3. Effect of atomic oxygen on resistance of nickel oxide crystal.

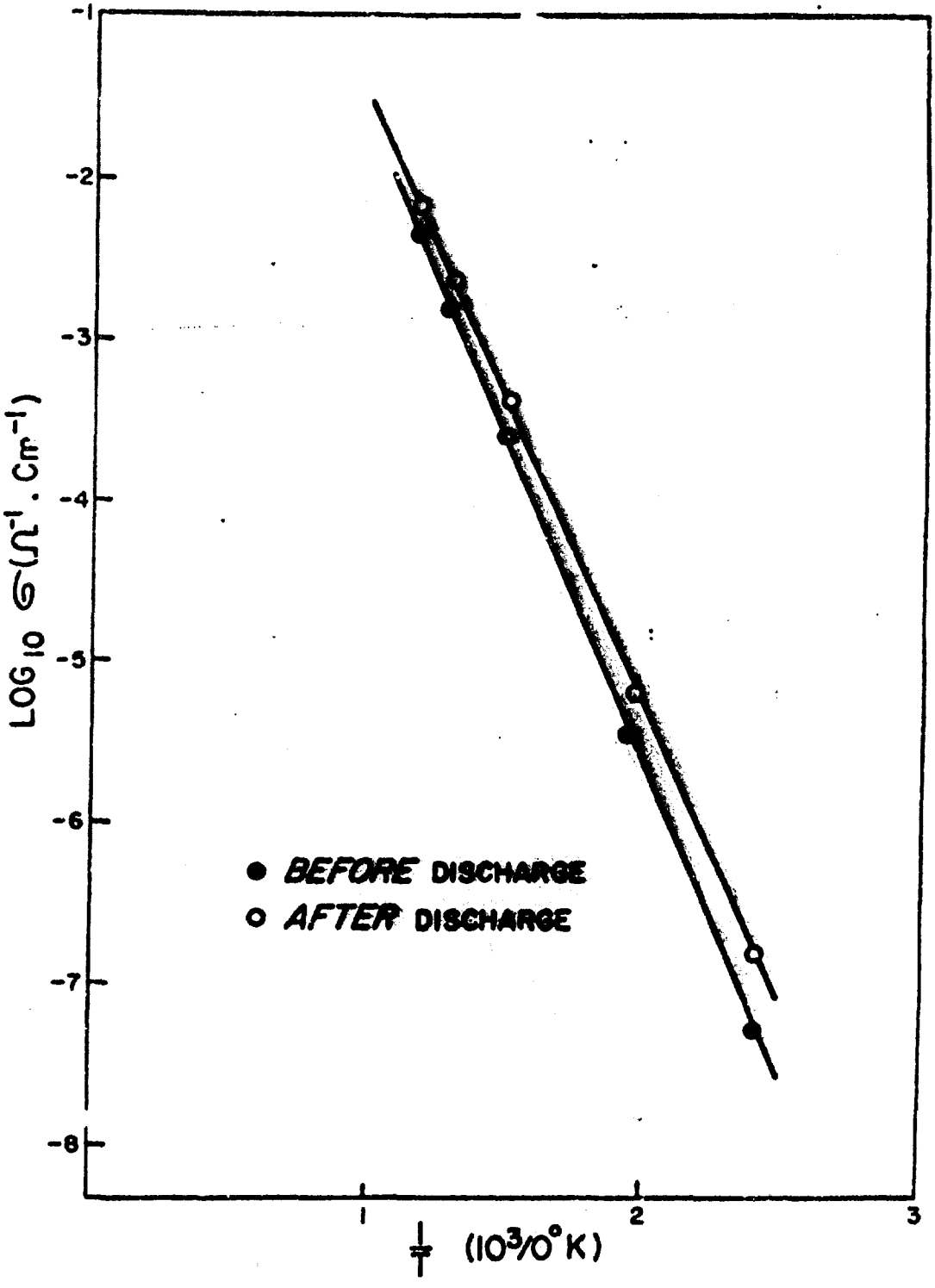

Fig. 4. Temperature dependence of conductivity of nickel oxide before and after exposure to atomic oxygen.

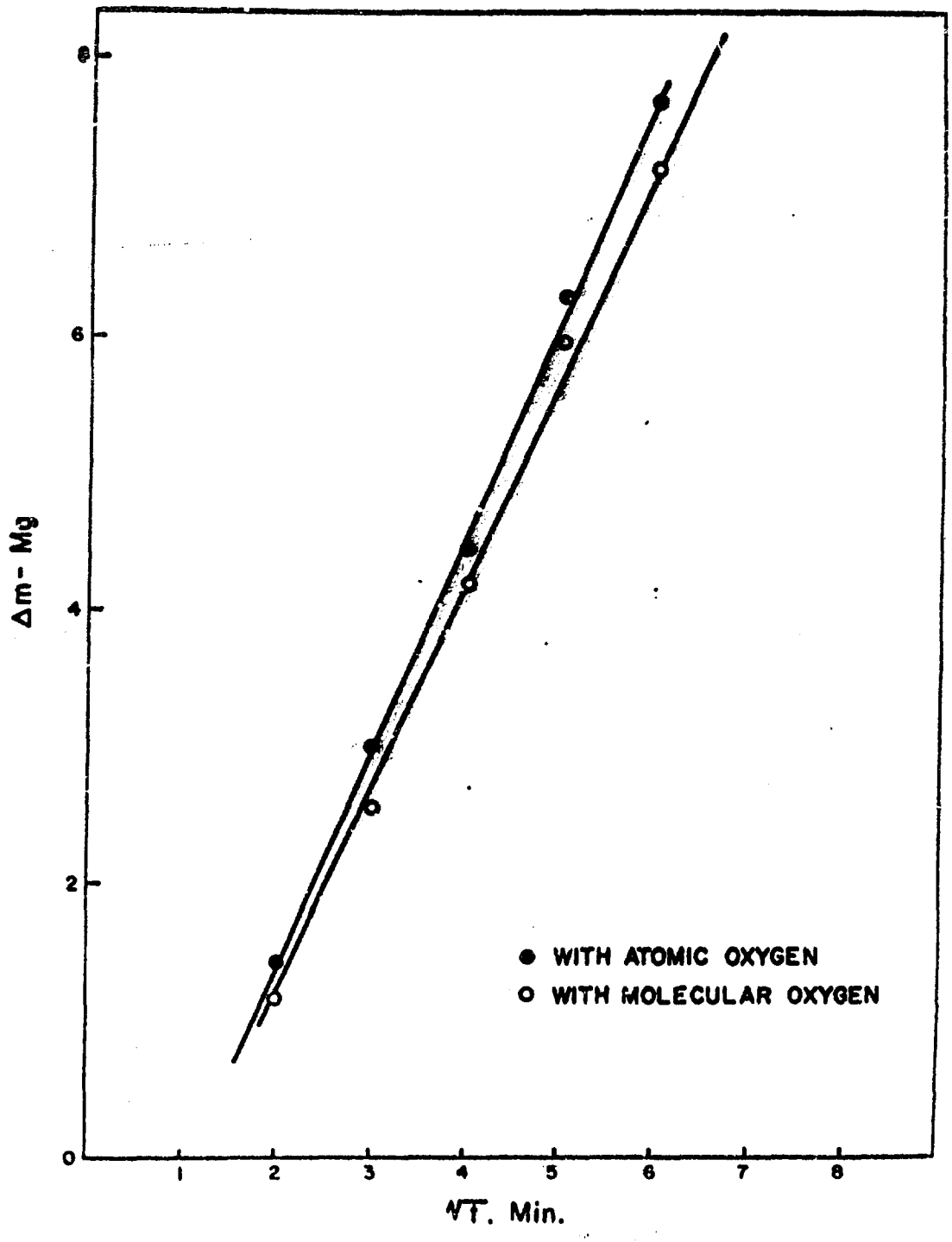

Fig. 5. Effect of atomic oxygen on oxidation of copper foil at 950° C.

A SELF SUSTAINING DIPOLE DISCHARGE IN OXYGEN

Nguyen Trinh Dzoanh/
Chemistry Laboratory, Indiana University, Bloomington

ABSTRACT

Two parallel metal electrodes are covered with porous insulating layers and immersed in oxygen at one atmosphere pressure. A dc potential difference of about 15 kV is applied between the plates, which are several cm apart. When a 100 microcurie alpha-particle source (Polonium-210) is introduced between the plates, an electric discharge is initiated which continues for one to two hours after the source is withdrawn. This discharge is called the self-sustaining dipole discharge. Its origin is believed to be a Malter effect occurring simultaneously at both electrodes, and caused by microspark discharges in the pores of the insulating layers. This mechanism is supported by the observation that tiny particles of insulating material may be ejected during the discharge.

/ Present address: Department of Physics, Illinois Institute of Technology, Chicago.

A SELF SUSTAINING GLOW DISCHARGE IN OXYGEN

Nguyen Trinh Doanh
Chemistry Laboratory, Indiana University, Bloomington

The simplest form of self sustaining discharge in gases is that between two parallel flat metal plates. When a dc potential is applied between two plates, the transformation of the gas from an insulator into a conductor may take place in various ways, depending on the pressure and the temperature of the gas. In ordinary air at atmospheric pressure and room temperature, as soon as the breakdown potential is attained, only a spark is produced. The originally very high resistance of the gas becomes suddenly a very low resistance of the order of one ohm. Persistent intermediate values of resistance cannot be realized, and the discharge is not self sustained.

The main reason for the absence of a self sustaining discharge in such a case is likely to be the fact that at high pressure the collision frequency of particles is high and the rate of energy loss is correspondingly high. The positive ions are then not sufficiently energetic to release from the cathode by ionic impact electrons necessary to maintain the discharge.

The well known classical way to maintain the discharge between the two plates is to increase the positive ion energy by reducing the pressure of the gas to a few millimeters of mercury, thereby minimizing the collision frequency of the particles. The discharge current at low pressure is given by the Townsend relation

$$i = i_0 \frac{e^{ad}}{1-\gamma(e^{ad}-1)} \qquad (1)$$

in which a is the first Townsend coefficient, defined as the number of electrons produced in the path of a single electron traveling a distance of one centimeter in the direction of the field. d is the distance between the two electrodes, γ is the second Townsend coefficient due primarily to the ionic impact. i_0 is the current produced by an external source,

such as cosmic rays, etc.

It is proposed to discuss another method to maintain a discharge between two parallel plates without decreasing the pressure, and to try to generalize it to any geometric configuration.

BASIC PRINCIPLES

At relatively high pressure, the discharge between two parallel plates cannot be self sustaining because of the lack of the second ionization coefficient γ. If an artifice is introduced that can produce this second ionization coefficient γ, even under some other form than that of ionic impact, the discharge will certainly be maintained.

This artifice can be found from a field effect known as the Malter effect.[1] When a metal target is covered by a layer of porous insulator - such as some metal oxides, dusts, organic compounds, etc. - and bombarded by a charged particle beam, an enormous electronic current can be drawn off from the target by the effect of the high field built up. This high-field effect stops when the incident charged particle beam is cut off. This phenomenon has also been observed by Guntherschulze,[2] who used a graphite and aquadag target covered by aluminum oxide particles and bombarded by positive ions. The electron emission was much higher when the oxide layer was present.

Although the target is bombarded by a charged-particle beam (ionic or electronic), the mechanism of this emission is completely different from the classical secondary emission. In the latter process, incident charged particles react with the conduction electrons of the metal target and the electrons can escape through the metal surface if the transfer of

---

[1] L. Malter, Phys. Rev. 49, 478 (1936).
[2] Guntherschulze, Physik [illegible], 778 (1933).

momentum to them is sufficient. In the present case, the oxide layer, generally a pretty good insulator at room temperature, prevents the electrostatic charges from flowing away and keeps them for a while on its surface. A gradient of potential is thus created, which increases quickly to a high value because of the small distance between the target and the charged insulator layer. Guntherschulze attributed the increase of electronic current to the surface field emission, due to the high gradient of potential built up in his experiment by the positive ions deposited on the surface of the aluminum oxide. Malter[3] used a target covered by an aluminum oxide film formed by anodic oxidation, and the target at ground potential was bombarded by an electronic beam. He suggested that when the incident electrons impinged upon the aluminum-oxide surface, the classical secondary electronic emission took place first, and the emitted electrons were immediately attracted to the collector. A positive charge was thus built up on the surface of the oxide film because of its high resistance and then field emission occurred.

There was, however, no published quantitative data to support the hypothesis about the built-up positive charge It seems likely from the experimental point of view that the phenomenon was governed by micro-spark discharges. When the potential at the surface of the porous insulating film in both cases (Malter and Guntherschulze) reaches the sparking potential of the ambient gas, a microdisruptive discharge occurs through the pores of the film, and the gas layer at the surface of the target becomes strongly ionized. This provides a multiplication of ions. The incident charged particle beam acts as an exciting source. The system target, porous insulator behaves as a mosaic of condenser which is charged by the incident charged beam and discharged

---

[3]L. Malter, Phys. Rev. 50, 48(1936).

through the pores of the insulator film. The charging and discharging times t_c and t_d depend on the capacity of the condensers, everything else being equal.

The charged particles so created thus reach the collector in pulses. The frequency of the charge and discharge of this group of condensers is very high, so that the collected current appears to be continuous. During the charging time t_c the collector does not receive any charge from the ionized gas. When the surface sparking potential is reached, the micro-discharge occurs, the electric field at the surface of the insulator layer is suddenly reduced to a small value. The gas layer is strongly ionized and the charge cycle will be repeated again and again. It is only during the discharging time that the collector can attract the charges from the plasma, depending on its polarity and potential.

Although the enchanced charge is largely due to the ionized gas, the extraction of charged particles from the target by field emission is also possible. If the field strength is high enough, however, this emission is assumed to be weak, compared to that from the ionization of the gas layer, since the electric field at the electrode surface is limited to the average value by the Paschen's law.

The photoelectric effect may also play a part in the production of ions. Radiation of short wave length, such as ultraviolet, should be abundant. The great amount of ozone created when the gas is air or oxygen may be good proof of the existence of such radiation.

The emission by ionic impact is not negligible, because the charged particles in the gap can be accelerated by a high field which reaches several thousand volts per centimeter. Projection of charged material particles from the target would be expected, and is in fact often observed.

With the concept of the condenser in mind, the value of the voltage built up and the field strength at the electrode surface can be estimated. The porous insulating film is considered to be approximately a monolayer of spheres of radius a and (Fig. 1) the contact of an insulating sphere with a plane is assumed to be limited to the area where the gap is less than a certain fixed distance. The area of contact will be proportional the square of diameter of sphere d^2, and the resistance of the area of contact to $\rho d/d^2 = \rho/d$, where ρ is the resistivity of the material. The ionic current to the sphere will be proportional to $d^2 i$. The voltage built up will therefore be

$$V_B = K(\rho/d)\ d^2 i = Kdi\rho$$

where K is a constant. If we consider the surface of the condenser (charged sphere target) as reduced to the area of contact and a great part of charges concentrated on the top of the sphere, the charge Q built up will be proportional to the ratio,

$$\frac{\text{area of contact}}{\text{gap of the small condenser}}$$

and to the voltage V_B.

$$Q = \frac{d^2}{d} V_B = Aid^2\rho$$

A is a coefficient of proportionality.

The electric force on this charge will be

$$F = AEid^2\rho, \qquad (2)$$

where E is the electric field near the surface of the target and i is the incident beam intensity.

It appears that the formula (2) given a possibility for measuring E if we can measure F which tends to apply the insulating film strongly to the target. This fact was clearly demonstrated by experiment.

The formula shows that the voltage built-up depends on the thickness

Porous dielectric film on metal electrode

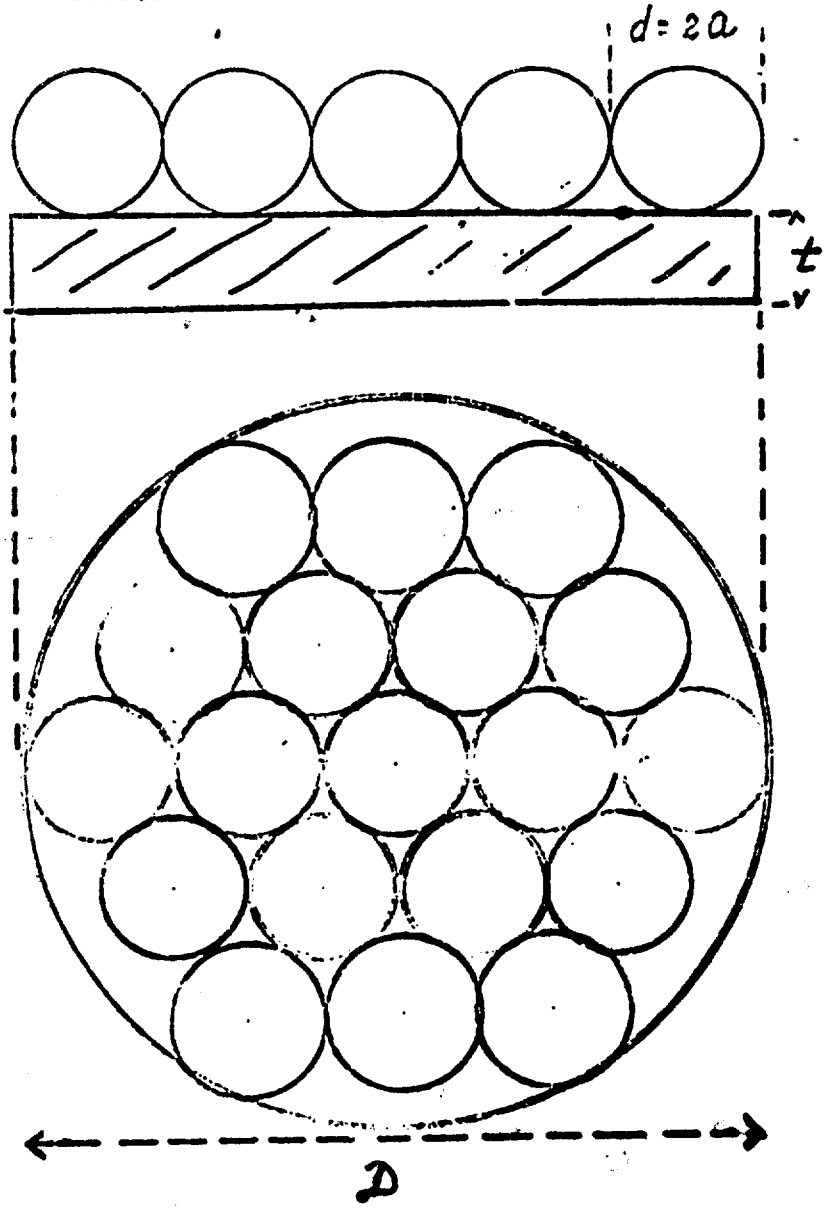

t = metal electrode thickness

D = electrode diameter

//// = Metal

d = dielectric sphere diameter

a = radius of dielectric sphere

and resistivity of the insulating film and the incident beam intensity. If the thin film is compact, the voltage V must reach a high value in order to create a microspark discharge through the insulator thickness. In that condition, the Malter effect would not easily occur; on the contrary, for porous insulating films such as certain oxides, dust etc., the disruptive voltage is rather low through the gas located in the pores in comparison with that through the solid. Therefore, the disruptive microdischarge can take place relatively easy and the residual gas will be immediately ionized. As discussed above, the phenomenon is probably governed by the Paschen's law. For a given gap between the target and the charged insulator film, the microdiruptive discharge takes place much easier at the pressure which corresponds to the minimum of the Paschen curve.

Self Sustaining Dipole Discharge at High Pressure

Now, instead of a cylindrical collector, two targets, both covered by a porous insulating film, are put one in front of the other. The pressure of the gas is about one atmosphere or higher. If these two parallel plates are bombarded at the same time by a charged particle beam from an external source, the Malter effect mentioned above must occur simultaneously in the two opposite surfaces.

For this purpose, a source of polonium 210 of two hundred microcuries, deposited on the top of a small glass rod, was placed in the interelectrode space and a dc potential applied between the two electrodes. The alpha particles, having an energy of 5.3 MeV, will create a strong ionization of the gas. In air, for example, at atmospheric pressure, they are able to produce 1.5×10^{3} ions per centimeter of path. Under the influence of the difference of dc potential, the cloud of electrons is accelerated and produces

other ion pairs.

The positive and negative particles so created are accelerated by the dc electric field in opposite directions toward the insulator films which cover the two electrodes. The local electric field is progressively built up at the films until the sparking potential is reached. The microdisruptive discharge is then brought about through the pores of the insulator films of both sides. For a symmetrical geometry, such as two parallel plates, it is likely that the Malter effect takes place quicker on the positive electrode than on the negative one because of the high mobility of electrons, despite of the fact that the sparking potential in a gas is slightly higher in the negative than in the positive polarity. When the microdischarge occurs simultaneously in both sides, it is no longer necessary to maintain the discharge by a polonium source. The discharge becomes self sustaining. Each electrode serves as an ion source for the other. Two electric currents of opposite polarity flow in the electrode interspace in opposite directions and supply successive buildups of charges for the two electrode surfaces. In order to express the processes of ion production at the two opposite electrodes, it is proposed to call this discharge a <u>Self Sustaining Dipole Discharge</u> (S.S.D.D.)

At the outset of the S.S.D.D. there is always a sudden potential drop. This phenomenon is interesting in itself and appears to have a clear analogy with the self sustaining discharge in a gas photoelectric cell which, once started, can be maintained without incident exciting light. The porous insulator film in the S.S.D.D. plays the same role as the sensitive surface of the photoelectric cell, except that the mechanism of ion production is quite different.

Thus the self sustaining discharge can be maintained between two parallel plates at high pressure (atmospheric pressure or more) owing to the porous

insulation at the surfaces of the electrodes. This provides a secondary Townsend coefficient γ which is necessary to maintain the discharge but does not exist at high pressure when the electrodes are bare.

The polonium source is particularly useful in effecting the first strong avalanche of charged particles. The current i_o in the formula

$$i = \frac{i_o e^{ad}}{1-\gamma(e^{ad}-1)}$$

is then high enough to furnish the necessary charges to start the micro-discharge process at the electrode surfaces.

Theoretical Study of the Potential and Field Distribution

In order to understand the behavior of such a discharge, it is interesting to know the modification of the electrostatic field due to the presence of the space charge p formed by the cloud of ions of both signs.

$$p = p_{(+)} - p_{(-)}$$

The problem is naturally governed by the Maxwell equations. At first it is assumed that the ionic recombination is negligible owing to the high velocity of ions and that the variation of the magnetic field due to the ionic flow is also negligible, because of the stationary state.

These considerations being taken into account, the Maxwell equations can be written:

$$\text{div } \vec{E} = 4\pi(p_{(+)} - p_{(-)}) \qquad (3)$$

$$\text{curl } \vec{E} = 0$$

$$\text{div } \vec{j} = 0$$

in which $\vec{E}$ is the electric field during the discharge, $p_{(+)}$ and $p_{(-)}$ are, respectively, the density of space charge due to the ions of both signs. The density of the current is j. As curl $\vec{E} = 0$, we can write

$$\vec{E} = - \vec{\text{grad}}\ \Phi \tag{4}$$

in which Φ is the corresponding potential.

The velocity of the positive and negative ions is given by

$$v_{(+)} = k_{(+)}E,\ v_{(-)} = k_{(-)}E$$

where $k_{(+)}$ and $k_{(-)}$ are, respectively, the mobilities of the positive and negative ions. Then we can write the expression for the density of current $\vec{j}$

$$\vec{j} = \left[p_{(+)}k_{(+)} + p_{(-)}k_{(-)} \right] \vec{E} + D_{(+)}\vec{\text{grad}}\ p_{(+)} + D_{(-)}\vec{\text{grad}}\ p_{(-)} \tag{5}$$

in which $\underline{D}$ is the diffusion coefficient of two kinds of ions. The conservation of ionic flux represented by the equation (3) will then be expressed as follows.

$$\text{div}\ \vec{j} = \text{div}\ \beta \vec{E} + D_{(+)}\ \Delta p_{(+)} + D_{(-)}\ \Delta p_{(-)} = 0 \tag{6}$$

in which $\beta = p_{(+)}k_{(+)} + p_{(-)}k_{(-)}$, or, after developing div $\beta \vec{E}$, one has

$$\beta\ \text{div}\ \vec{E} + \vec{E}\ \vec{\text{grad}}\ \beta + D_{(+)}\Delta p_{(+)} + D_{(-)}\Delta p_{(-)} = 0 \tag{7}$$

In order to have the general equation of the field and potential distribution for the S.S.D.D. in any geometric configuration, the value of $p_{(+)}$ and $p_{(-)}$ in (6) must be expressed. Equation (3) is not sufficient; a new factor is going to be introduced which can be, at least, determined by experiment.

The total discharge current is given by

$$I = I_{(+)} + I_{(-)} \tag{8}$$

$I_{(+)}$ and $I_{(-)}$ are the positive and negative ionic currents. The conservation of current components can be expressed as follows

$$I_{(+)} = S\left[p_{(+)}k_{(+)}E + D_{(+)}\text{grad}\ p_{(+)} \right]$$

$$I_{(-)} = S\left[p_{(-)}k_{(-)}E + D_{(-)}\text{grad}\ p_{(-)} \right].$$

This ratio $I_{(+)}/I_{(-)}$ is equal to:

$$I_{(+)}/I_{(-)} = \frac{p_{(+)}k_{(+)}E + D_{(+)}\text{grad}\ p_{(+)}}{p_{(-)}k_{(-)}E + D_{(-)}\text{grad}\ p_{(-)}} \cdot \tag{9}$$

In general, the velocity of ions due to the thermal diffusion is negligible in comparison with that due to the electric field. The diffusion terms have an insignificant influence on the value of the ratio (9) which can be written as

$$\frac{I_{(+)}}{I_{(-)}} = \frac{p_{(+)}k_{(+)}}{p_{(-)}k_{(-)}} = g \tag{10}$$

If attention is focused on the negative electrode side, $I_{(+)}$ will be called the excitor current and $I_{(-)}$, the inductor current, and vice versa on the positive electrode side. $I_{(+)}$ and $I_{(-)}$ have a mutual action, one on the other. The ratio, $g = p_{(+)}k_{(+)}/p_{(-)}k_{(-)}$, can be called a production or multiplication factor and can be measured by the probe method, for example. This ratio will play the role of the second Townsend coefficient γ in the discharge at low pressure.

Now from equations (3) and (10) the value of $p_{(+)}$ and $p_{(-)}$ can be deduced

$$\begin{aligned} &\text{div } E = 4\pi(p_{(+)} - p_{(-)}) \\ &g = \frac{p_{(+)}k_{(+)}}{p_{(-)}k_{(-)}} \\ &p_{(-)} = \frac{\text{div } \vec{E}}{4\pi}\left(\frac{g\,k_{(+)}}{g\,k_{(-)} - k_{(+)}}\right) \\ &p_{(+)} = \frac{\text{div } \vec{E}}{4\pi}\left(\frac{g\,k_{(-)}}{g\,k_{(-)} - k_{(+)}}\right) \end{aligned} \tag{11}$$

Equation (7) will then become:

$$\frac{\text{div } \vec{E}}{4\pi}\left(\frac{g\,k_{(-)}k_{(+)} + k_{(+)}k_{(-)}}{g\,k_{(-)} - k_{(+)}}\right) + \vec{E}\,\text{grad}\left(\frac{g\,k_{(-)}k_{(+)} + k_{(+)}k_{(-)}}{g\,k_{(-)} - k_{(+)}}\right)\frac{\text{div } \vec{E}}{4\pi}$$
$$+ D_{(+)}\Delta\left(\frac{\text{div } \vec{E}\,g\,k_{(-)}}{4\pi(g\,k_{(-)} - k_{(+)})}\right) + D\Delta\left(\frac{\text{div } \vec{E}\,k_{(+)}}{4\pi(g\,k_{(-)} - k_{(+)})}\right)$$

$$= 0 .$$

After simplification and the introduction of $E = -\ \text{grad}\ \Phi$, one obtains (12)

$$(\Delta\Phi)^2 + \vec{\text{grad}}\ \Phi\ \vec{\text{grad}}\ (\Delta\Phi) = \Delta(\Delta\Phi)\ \frac{g\ D_{(+)}k_{(-)} + D_{(-)}k_{(+)}}{k_{(+)}k_{(-)}\ (g+1)} \qquad (12)$$

It is interesting to notice that if $g = 1$, this means that $p_{(+)}k_{(+)} = p_{(-)}k_{(-)}$, and the coefficient of the second member of the equation (12) can be written:

$$\frac{D_{(+)}k_{(-)} + D_{(-)}k_{(+)}}{2\ k_{(+)}k_{(-)}}\ .$$

If this expression is multiplied by

$$\frac{k_{(+)} + k_{(-)}}{k_{(+)} + k_{(-)}}$$

it becomes:

$$\frac{D_{(+)}k_{(-)} + D_{(-)}k_{(+)}}{k_{(+)} + k_{(-)}}\ .\ \frac{k_{(+)} + k_{(-)}}{2k_{(+)}k_{(-)}}$$

It is clear that this expression is equal to $D_a/2k$ in which

$$D_a = \frac{D_{(+)}k_{(-)} + D_{(-)}k_{(+)}}{k_{(+)} + k_{(-)}}$$

is a classical ambipolar diffusion coefficient and $k = \frac{k_{(+)}k_{(-)}}{k_{(+)} + k_{(-)}}$ is a reduced mobility coefficient. The general equation which governs the potential and field distribution will be:

$$(\Delta\Phi)^2 + \vec{\text{grad}}\ \Phi\ \vec{\text{grad}}\ (\Delta\Phi) = \frac{D_a}{2k}\ \Delta(\Delta\Phi)$$

If the space charge is neutral,

$$p = p_{(+)} - p_{(-)} = 0 \text{ and } \left(g = \frac{k_{(+)}}{k_{(-)}}\right)\ .$$

The concentration of electrons and positive ions is equal, the densities of current due to charge carriers are proportional to the ratio of mobilities.

the current is then almost all carried by electrons. In fact, if $p_{(+)} = p_{(-)}$, one obtains

$$\alpha = \frac{p_{(+)}}{p_{(-)}} \frac{k_{(-)}}{k_{(+)}} = \frac{k_{(-)}}{k_{(+)}} \quad \text{by definition.}$$

As $k_{(-)} \gg k_{(+)}$, the coefficient of the second member of equation (12) can be written:

$$\frac{\frac{k_{(+)}}{k_{(-)}} D_{(+)} k_{(-)} + D_{(-)} k_{(+)}}{k_{(+)} k_{(-)} \frac{k_{(+)} + k_{(-)}}{k_{(-)}}} \simeq \frac{D_{(+)} + D_{(-)}}{k_{(+)} + k_{(-)}} \simeq \frac{D_-}{k_-} \tag{13}$$

The ionic temperature is much smaller than the electronic temperature, so $D_{(+)} \ll D_{(-)}$. The expression (13) is then reduced to $D_{(-)}/k_{(-)}$. Therefore, the general equation for field and potential distribution in the positive column, where $p_{(+)} = p_{(-)}$, is only modified by the electronic diffusion.

$$(\Delta\phi)^2 + \vec{\text{grad}}\,\phi\ \vec{\text{grad}}\,(\Delta\phi) = \lambda(\Delta\phi)\,\frac{D_{(-)}}{k_{(-)}} .$$

However, the thermal agitation is in general so small that we can afford to neglect it in certain cases, such as in air at atmospheric pressure and room temperature. Then,

$$(\Delta\phi)^2 + \text{grad}\,\phi\ \text{grad}\,(\Delta\phi) = 0 .$$

After integrating this equation taking into account the boundary conditions, other interesting factors can be deduced from the expression for ϕ, such as the field, the space charge distribution, etc. But the differential equation with fourth order partial derivative cannot be solved in the classical way. It is necessary to use approximation methods and a computer. If the mathematical difficulty prevents one from going farther in this study, it is, however, quite possible to measure the space potential, and the electric field will be obtained by simple graphical integration.

EXPERIMENTS

The experimental apparatus is shown in Figure (2). The electrodes are held by two carriages of plexiglass which can slide on a pair of rails. They are lodged in an aluminum box which is connected to the conventional pumping system through a valve. The carriage can be moved from outside by a gear system, so that the distance between electrodes can be varied and determined easily. For reason of convenience, a fiberglass cloth is used in lieu of the oxide layer. This cloth had a thickness of 0.10 mm and was woven of 0.007 mm fibers. The resistivity of the glass is comparable with that of oxide and the porosity can be evaluated by an ordinary microscope. The hygroscopic nature of the glass reduces the resistivity of the insulating layer to so small a value that the discharge is difficult to initiate, but a small increase in temperature is enough to eliminate this problem. The glass cloth which plays the role of oxide layer is held by two concentric plexiglass rings of diameter twice that of the electrodes. The outside diameter of one plexiglass ring is nearly equal to the inside diameter of another. The glass cloth is located between them.

In order to avoid the nonuniform field at the edge of the electrodes, a metal guard ring was used. The electrodes of 1.25 cm diameter are made of pure metal (copper or aluminum). The electrical circuit is shown in the diagram.

The top of a glass rod carrying a polonium source of 200 microcuries can be moved in or out of the interelectrode space by manipulation from outside the box. The temperature in the box is measured by a copper constantan thermocouple and the pressure by a thermocouple gauge and a mercury column.

Tank oxygen furnished by Matheson Company was used without purification. The gas was heated slightly by a resistance before being admitted to the experimental box.

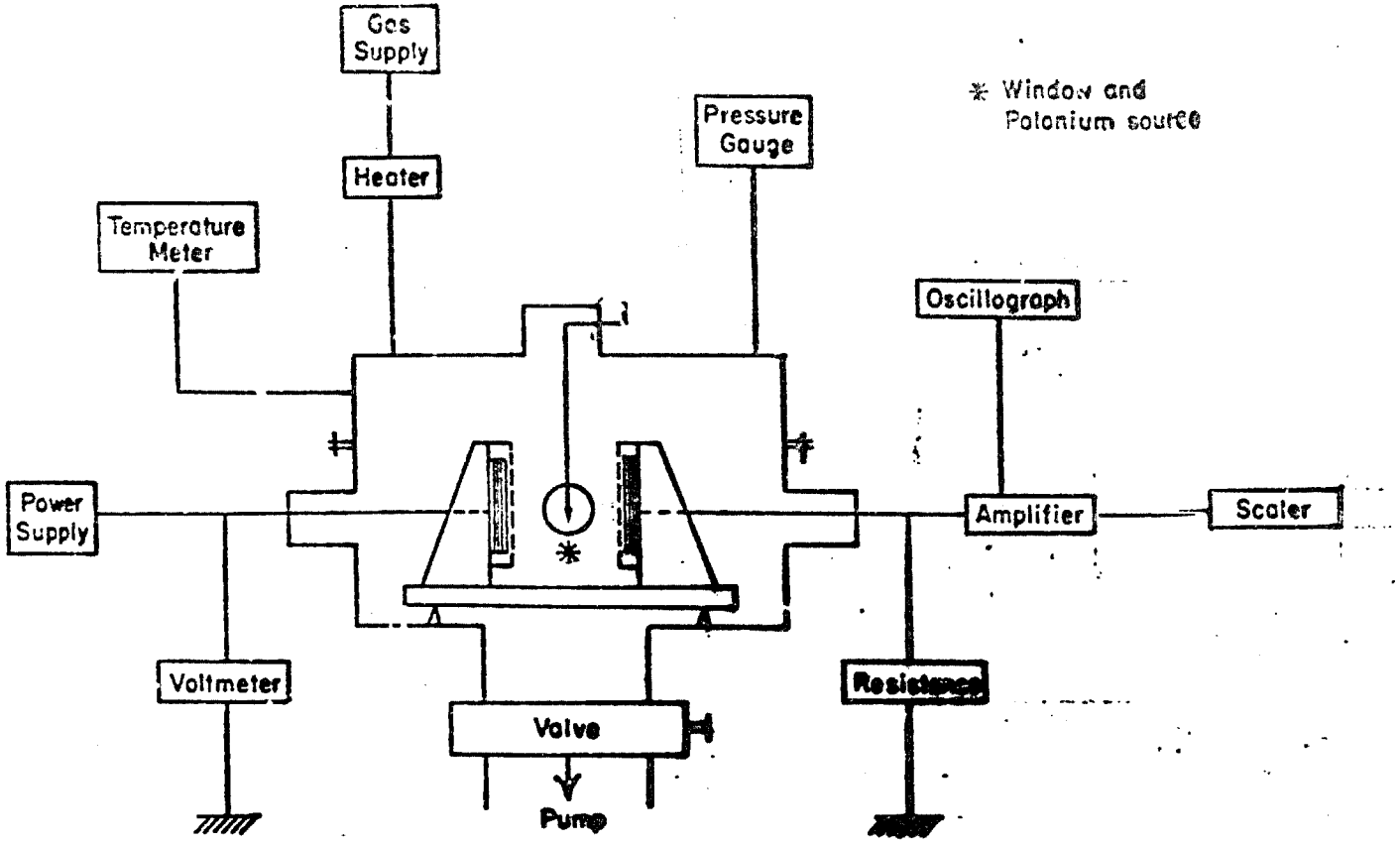

FIGURE 2

Experimental apparatus for self-sustained dipole discharge.

Onset of the S.S.D.D. The air in the box was evacuated before admitting the slightly warm oxygen above up to one atmosphere or more. A dc potential of about 1 KV was applied between two electrodes, both covered by a porous insulating film. As soon as the excitor alpha source was put into the inter-electrode space, a permanent discharge current was obtained. Both covered electrode surfaces were suddenly illuminated. The luminosity was much brighter on the cathode than on the anode. This fact may be due to the heavy bombardment by positive ions. The polonium source was then removed but the discharge continued between two parallel electrodes under a pressure of one atmosphere or more.

The minimum voltage between electrodes, necessary to start the S.S.D.D. depends on the gas pressure and on the gas temperature, for a given geometric configuration. This result apparently confirms the foregoing explanation that the mechanism of the Malter effect, in this instance at least, is governed by microsparks between the charged insulating film and the metal surface since it is entirely dominated by Paschen's law. The initiation time of the S.S.D.D. for a given applied voltage depends on the intensity of the excitor source and on the specific resistivity of the insulating film. If the ambient gas is loaded with water vapor, the initiation time is much longer, and sometimes the S.S.D.D. does not occur no matter how high the applied electric field may be, since the adsorbed water vapor reduces the resistivity of the insulating film to such a low value that the built up electrostatic field at the electrode surface is not high enough and therefore the microspark cannot take place.

If the experimental vessel is closed, the discharge current decreases slowly, and there is an increase in time in the quantity of ozone, and even some nitrogen oxide is formed in small amount owing to the presence of

attached to oxygen in the gas. In order to keep the discharge current constant, the applied voltage is increased slightly but almost continuously. After about two hours, the gas was warmed and the discharge stopped completely. This fact seems to be anomalous since in warm gas the mobility of particles is higher and the discharge current should be greater.

The formation of oxide layers, especially at the anode, has some influence on the discharge current in the S.S.D.D. but the presence of a great amount of ozone may also be a factor. It is well known that ozone produced by a dc discharge can reach approximately 30 per cent of the total gas volume. It was for a long time suspected that these gas molecules become heavy ions and move very slowly because of their mass toward the electrodes. When the gas in the experimental vessel was saturated with ozone and the current discharge was reduced to zero, the reinitiation of the S.S.D.D. could be effected by again using the polonium source at a higher applied voltage, but the discharge did not last very long (a few minutes). It was decided, therefore, to renew the gas continuously. In order to maintain the discharge current at certain given value, a weak flow of oxygen was arranged through a small leak through the valve which separated the pump and the experimental vessel. This small and continuous leak balanced the gas input and the pressure in the experimental box was thus kept constant. At a pressure of one atmosphere and with a polonium source of 200 microcuries, when a high voltage is applied to the electrodes, a certain time was necessary for the charges to build up on its surface, before the S.S.D.D. could start. This delay time for initiation of the S.S.D.D. depends on the value of the voltage and the distance between electrodes.

The variation of the applied voltage versus delay time is shown in Fig. [illegible] the interelectrode space being a parameter. It follows a

FIGU E 3

Dependence of delay time for initiation of S.S.D.D. on the applied voltage.

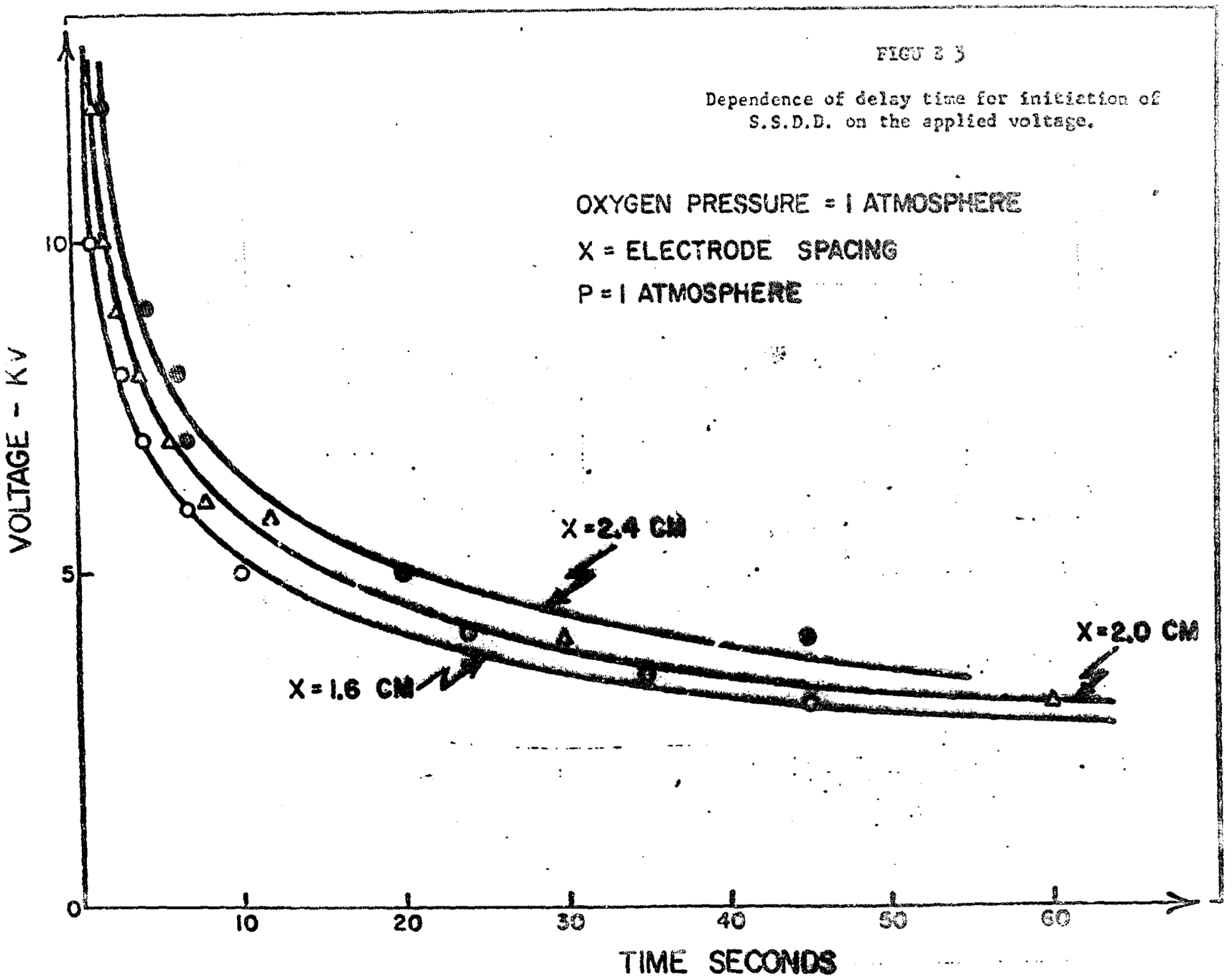

hyperbolic law. At high enough applied voltage the S.S.D.D. took place almost immediately. If the interelectrode space increased, more energy was necessary to start the S.S.D.D. for the same delay time. It is interesting to notice that the delay time increases linearly with the interelectrode space L for a given applied voltage as shown in Fig. (4). In fact; for a given working condition of temperature and pressure of gas, and resistivity of glass cloth, the breakdown voltage at the surface of the electrode should have a definite value. This value calculated above is given by:

$$V_B = kd\rho i$$

in which $i = SNeu$, u is the velocity of charged particles, e = electronic charge. S = surface area of electrode. N = number of charged particles, d and ρ are thickness and restivity of the glass cloth.

From these relations we have:

$$v = \frac{dx}{dt} = \frac{i}{SNe} = \frac{V_B}{SNek\rho d}$$

therefore

$$\int_o^L dx = \frac{V_B}{SNek\rho d} \int_o^t dt$$

$$L = \frac{V_B}{SNek\rho d}\ t \qquad (14)$$

This relation shows that the transit time t is proportional to the distance L between the two electrodes. It is reasonable to assume that the delay time τ is proportional to the transit time t of the charged particles across the electrodes.

$$\tau = Kt$$

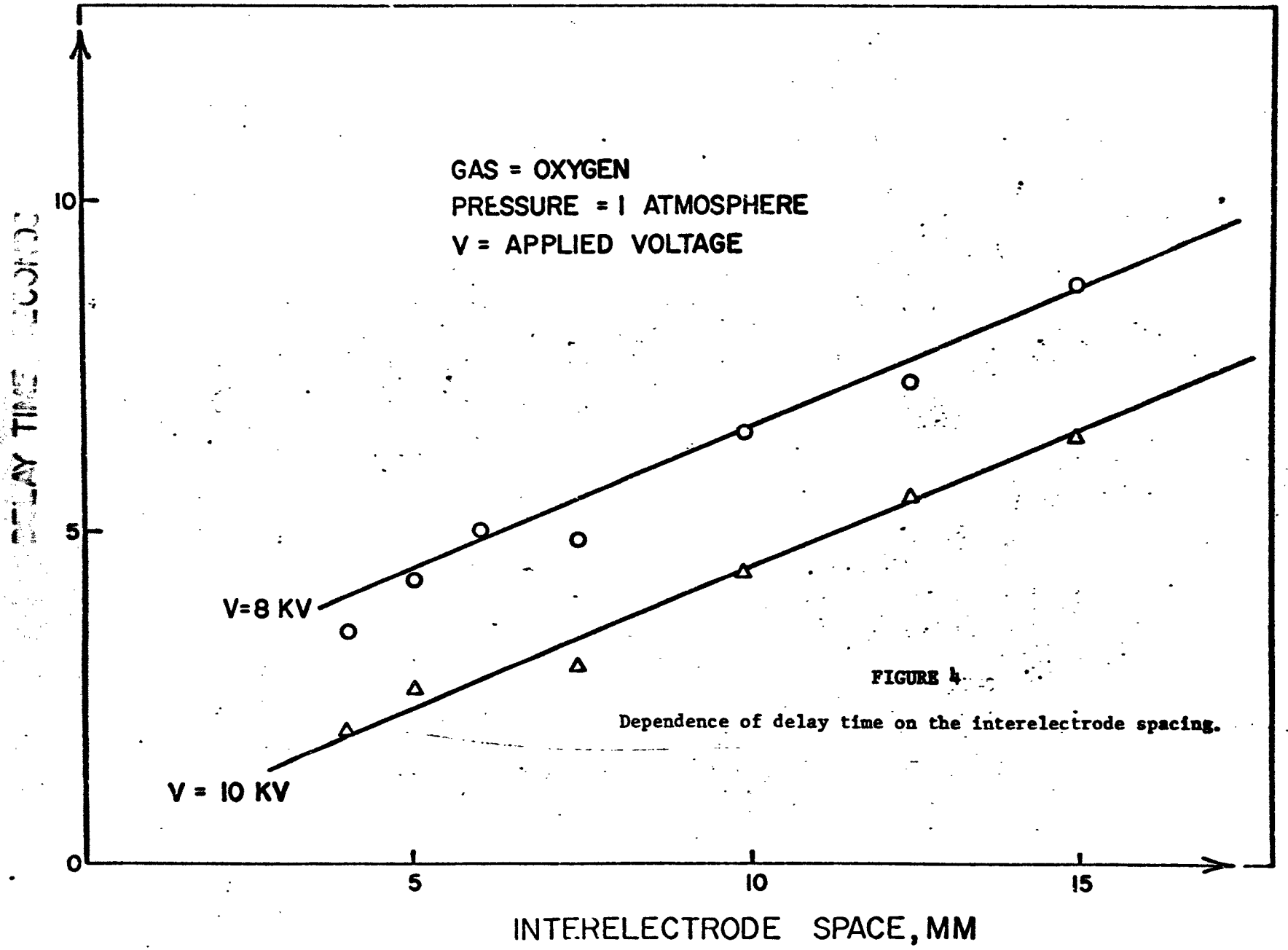

FIGURE 4

Dependence of delay time on the interelectrode spacing.

K is a constant of proportionality. The relation (14) becomes

$$L = \frac{V_B}{SNek_\varphi dK}\ \tau = AV_B\ \tau, \quad A = \frac{1}{SNek_\varphi dK} = \text{constant} \qquad (15)$$

This relation can explain the behavior of the curves in Figs. (3) and (4). In fact, the voltage built up at the surface V_B is a function of the applied voltage V. This function can be determined if the potential distribution is known, by solving the equation (12). Unfortunately the mathematical difficulty requires the use of the empirical relation between the discharge current i and the applied voltage V. This empirical relation deduced from the characteristic curve, $i = f(V)$, has the form: $i = MV^m$. (M and m are constants.) Since i is proportional to V_B as shown above, V_B is then proportional to V^m.

$$V_B \sim V^m$$

The relation (15) becomes:

$$L = A'V^m\ \tau$$

A' is a new constant of proportionality. For a given value of V, V_B is well defined and the delay time is proportional to the distance L of two electrodes as indicated by Fig. (4). If L is fixed, the applied voltage is given by

$$V = \left(\frac{L}{A'} \cdot \frac{1}{\tau}\right)^{\frac{1}{m}}$$

The variation of V and τ follows the hyperbolic law as indicated by the curve in Fig. (3). As one can see, all of these results fit the microbreakdown hypothesis previously discussed.

When the applied voltage and the interelectrode space are kept constant, the delay time variation in function of the gas pressure is shown in Fig. (5). The linearity is observed from low pressure up to about 65 mm Hg, then the

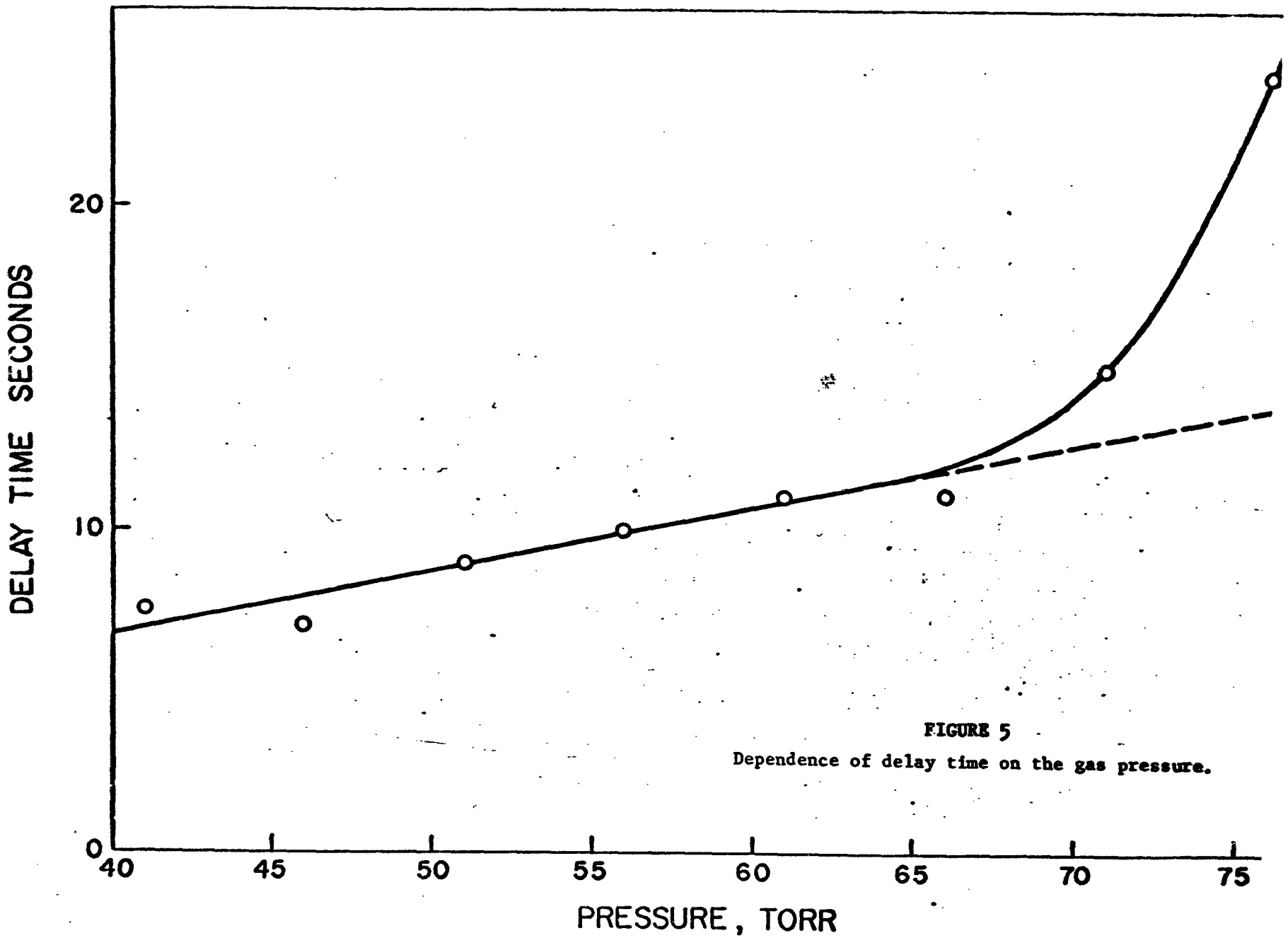

FIGURE 5

Dependence of delay time on the gas pressure.

delay time increased almost exponentially with the pressure. In fact, from the relation (15), the built up potential V_B is proportional to the discharge current i and therefore proportional to the mobility of the charged particles. Since the mobility is inversely proportional to the pressure, the delay time τ should vary linearly with the pressure as shown in the left part of the curve in Fig. (5). At the threshold of the S.S.D.D., the onset discharge current i being kept constant of about a few microamperes, the potential drop is then constant for a whole range of pressure, and is independent of the applied voltage for a given geometric configuration, as shown in the following Tables

Interelectrode space L (mm)	Applied Voltage V (kV)	Potential Drop ΔV (kV)	Pressure P mm Hg
24	3.5	0.05	76
24	3.5	0.05	71
24	3.5	0.045	66
24	3.5	0.05	56
24	3.5	0.055	41

Pressure P(atm)	Interelectrode space L (mm)	Applied Voltage V (kV)	Potential drop ΔV (kV)
1	40	6	0.2
1	40	7	0.2
1	40	8	0.2
1	40	9	0.24 (1)
1	40	10	0.35

(i) The onset current of the S.S.D.D. was slightly higher than the former value, therefore the potential drop was higher.

If the applied voltage is kept constant at a given pressure, the potential drop decreases as expected when the interelectrode space increases [see Fig. (5).]

Characteristic Curve of Current-Voltage of the S.S.D.D.

In order to characterize the self sustaining dipole discharge, it is necessary to know the variation of the discharge current i, when the applied voltage V between two electrodes increases, with different pressure as parameter. The graph Log (i) versus Log (V) is shown in Fig. (6). The parallelism of these graphs is quite clear. Therefore the variation of i as function of V follows the parabolic law. The equation of the graph is Log i = m Log V + Log M, hence:

$$i = MV^m \tag{16}$$

m is the slope of the graph Log (i) = Log (V) and is very close to 5.45 for oxygen. This coefficient depends probably on the nature of the gas. M is a constant which apparently depends on the pressure P of the gas. In fact:

$$\text{Log } i = m \text{ Log } V + \text{Log } M$$

Since the graphs parallel each other, the coefficient m is then constant for different pressures. If the potential V is kept constant the Log (M) = F(Log P) should have the same slope μ as the graph:

$$\text{Log } (i) - m \text{ Log } V = F(\text{Log } P)$$

since Log M = Log (i) - m Log V. For different values of V, one has different parallel curves. This slope μ given by the Fig. (7) is equal to -6.45 and the relation between M and P can be written

$$M = \text{constant} \times P^{-6.45} = \frac{C}{P^{6.45}}$$

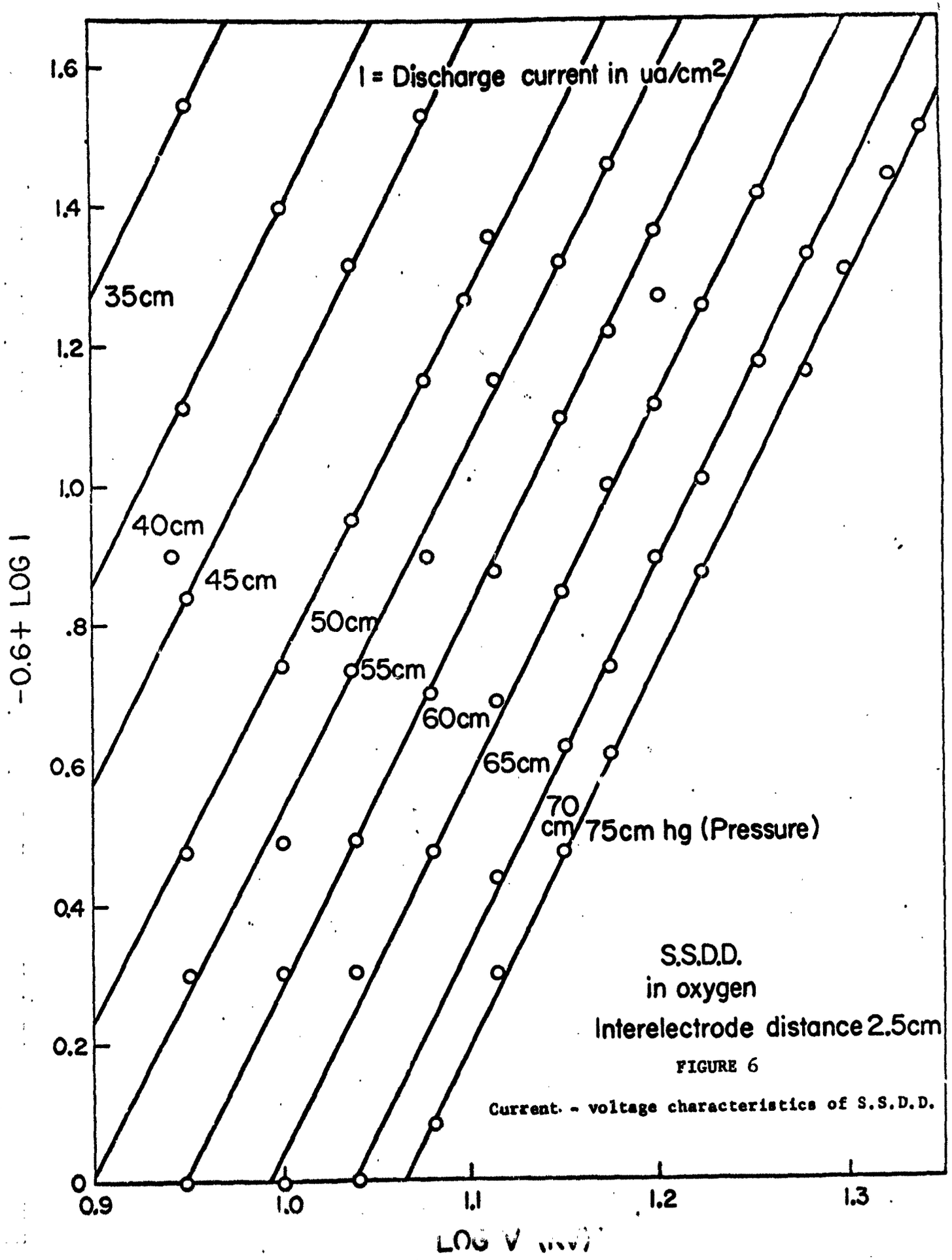

FIGURE 6

Current - voltage characteristics of S.S.D.D.

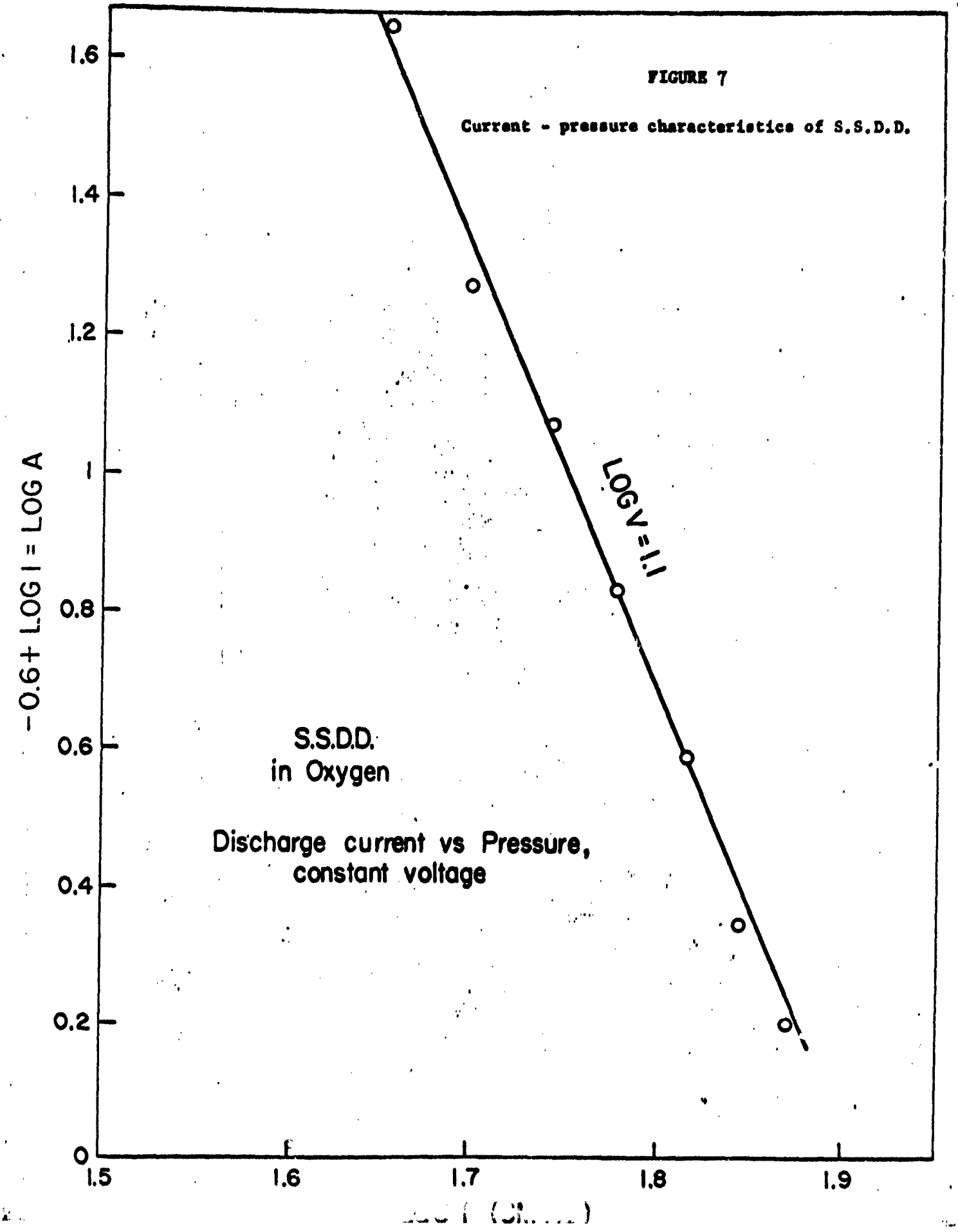

FIGURE 7

Current - pressure characteristics of S.S.D.D.

The relation (16) takes then the form

$$i = \frac{C\ V^{5.45}}{P^{5.45}} = \frac{C}{P}\ \left(\frac{V}{P}\right)^{5.45} \qquad (17)$$

Since the pressure P is inversely proportional to the mobility k of the charged particles, the relation (17) becomes

$$i = C\ \ k\ \left(\frac{V}{P}\right)^{5.45}$$

This is an empirical relation between i and V, deduced from the experimental graphs.

For a given applied potential, the discharge current decreases drastically if the distance between electrodes increases as shown in Fig. (8). From this series of curves, one can determine the necessary applied voltage between two electrodes in order to keep the discharge current constant as the distance increases.

Sparking Potential

It is widely recognized that the sparking potential between two metal electrodes depends upon the nature of the electrodes, especially when the latter are not clean. Decrease of the sparking potential with dusty or oxidized electrodes has been observed but the mechanism of this effect is not well understood and still subject to controversy. According to the results of this experiment it seems likely that the presence of oxide, dust or other porous insulators on the electrode surface will create a nucleus for a microspark at the surface, the obvious consequence of which is to start the main spark between two electrodes earlier than usual. The mechanism would be the same as that of a triggered spark gap described by

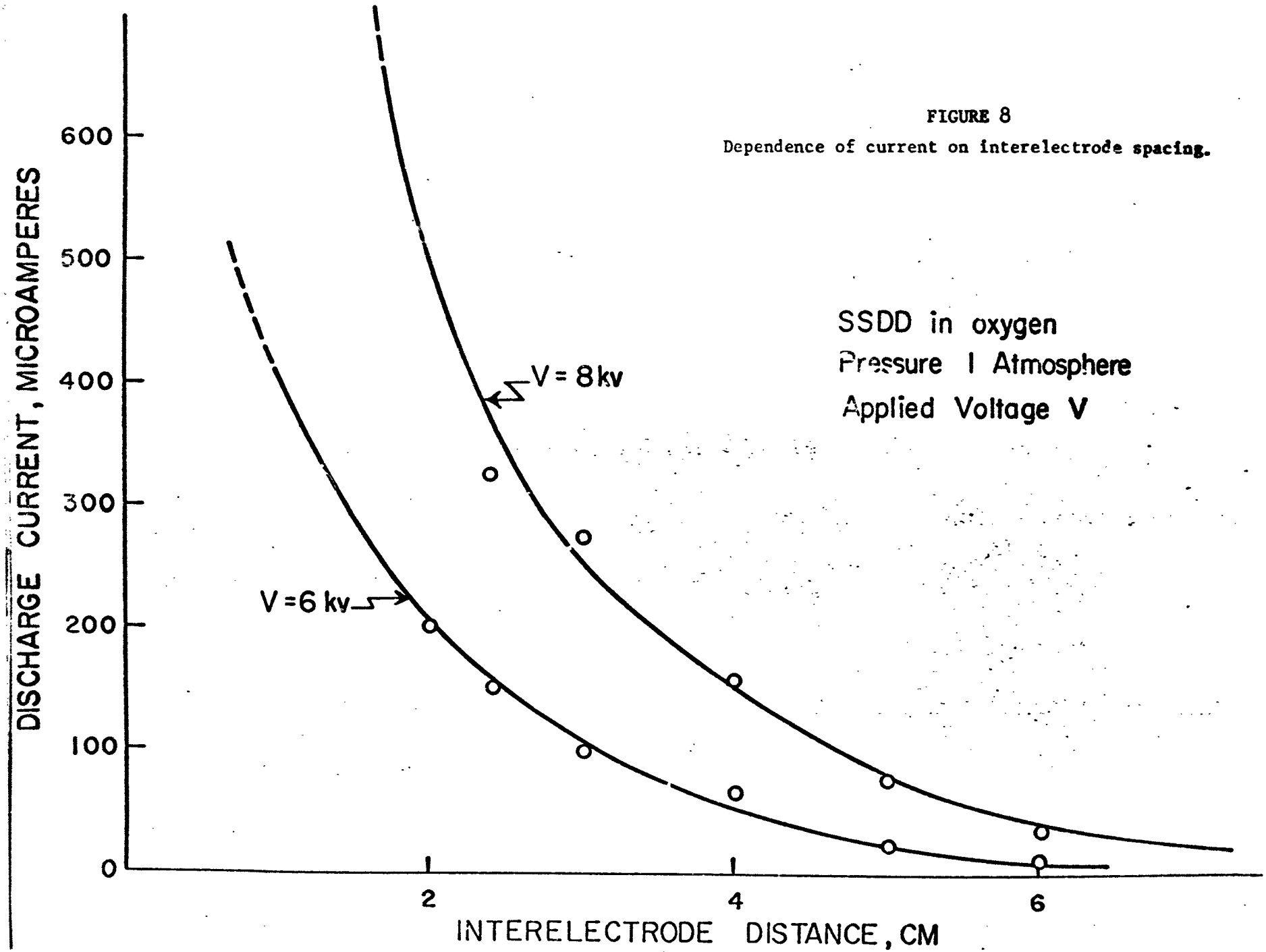

FIGURE 8

Dependence of current on interelectrode spacing.

Craggs et al.[4] in which the main spark is accelerated by a small spark generated by an auxiliary electrode. Figure (9) shows the variation of the sparking potential with pressure in three cases.

---

[4]Craggs, J. D., M. E. Haine and J. M. Meek, J. Inst Elect Engrs Pt. III A, 1946, 963.

FIGURE 9

Dependence of sparking potential on pressure.

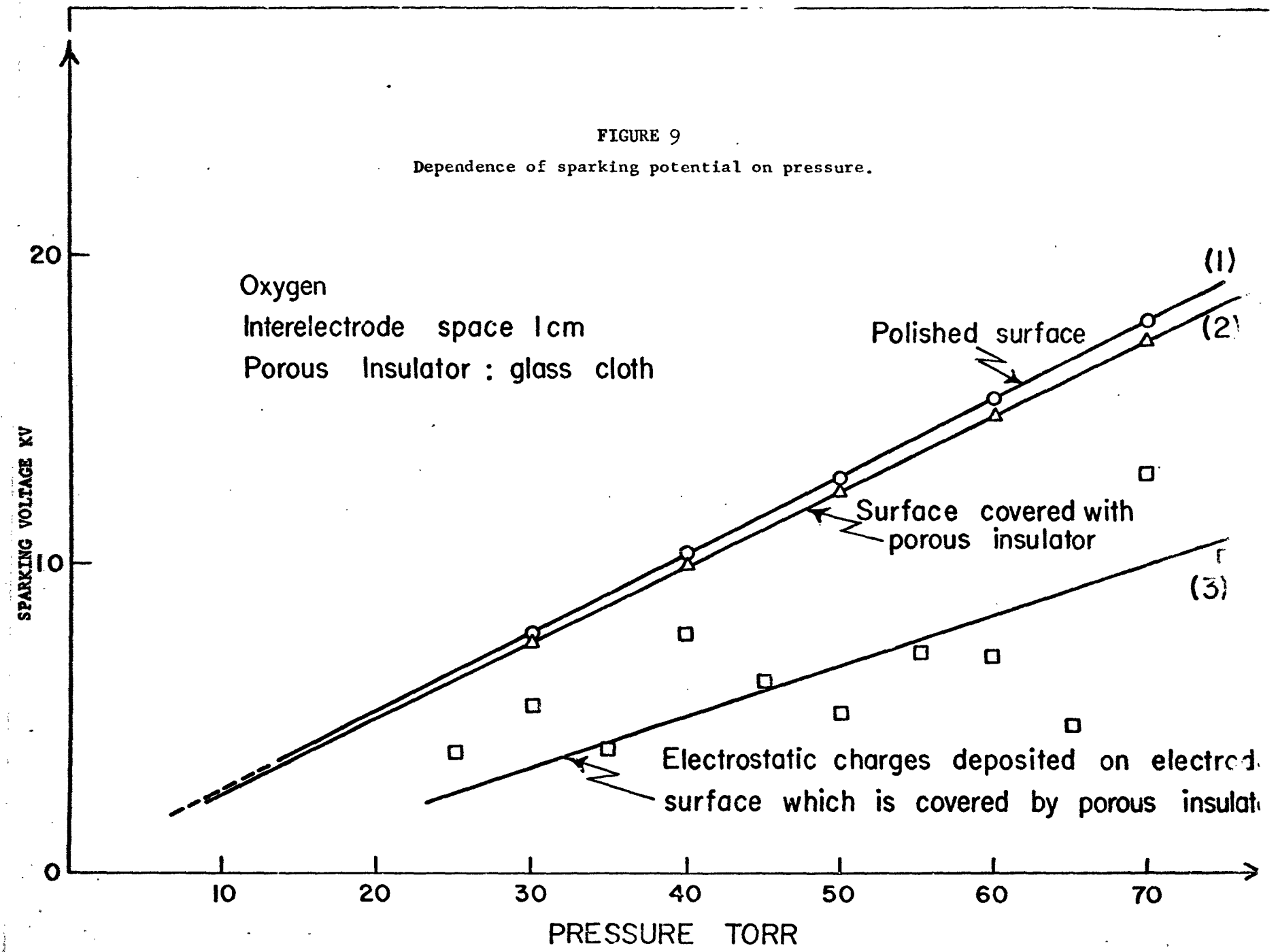

CORROSION OF METAL FILMS IN AN OXYGEN PLASMA AT HIGH PRESSURE

Jens Traetteberg, Nguyen Trinh Dzoanh, and Walter J. Moore
Chemical Laboratory, Indiana University, Bloomington

ABSTRACT

The oxidation of thin films of aluminum and copper by anodization in an oxygen plasma cell at one atmosphere and room temperature was studied by means of an electron microscope It appears that the oxide film formed by the oxygen plasma is torn into fissures by both electrical and thermal breakdown over the surface of the metal electrode. Selected area diffraction revealed the existence δAl_2O_3 with aluminum films and Cu_2O and CuO with copper films. Nucleation and growth of oxide below the outer surface of metal may be expected as a result of oxygen-ion bombardment from the plasma.

CORROSION OF METAL FILMS IN AN OXYGEN PLASMA AT HIGH PRESSURE

Jens Traetteberg, Nguyen Trinh Dzoanh, and Walter J. Moore
Chemical Laboratory, Indiana University, Bloomington

There has been a great increase in the use of gas plasmas, for example, in devices to study nuclear fission, in experimental ion propulsion engines, and in systems for carrying out specialized chemical reactions. Questions naturally arise concerning the effect of plasma atmospheres on metals and other materials of construction. One of the primary purposes of our O.A.P. contract was to study such processes. The successful development of the self sustaining dipole discharge provided a suitable means for such studies by making available a convenient oxygen discharge plasma at pressures of one atmosphere and above. This paper describes the observations made when metal films were exposed to anodic oxidation in this plasma.

Most metals are unstable at room temperature in contact with oxygen at atmospheric partial pressures. In the case of aluminum, a film of oxide about 25 Å thick is rapidly formed, separating the reactants. Further reaction can occur only by diffusion or migration of metal or oxygen ions through the film. Such transport thickens the film and therefore reduces the rate of reaction because of a decreased electrostatic field across the film. In order to increase this field and therefore its oxidation effect, the common method is to make the metal the anode in an electrolytic cell containing a suitable electrolyte. The physical structure of the oxide depends to a great extent on the electrolyte. In general a film thickness of a few thousand Angstroms can be obtained at room temperature.

It would be interesting to increase the gradient of potential at the metal surface under conditions similar to those in anodic oxidation but using, instead of liquid electrolyte, a gas already in the form of ions, commonly called plasma.

The recent successful development of the self sustaining dipole discharge[1] in our laboratory satisfied two conditions mentioned above (high surface electrostatic field and ionized gas) and provided therefore a new means for studying the oxidation of metals such as aluminum and copper in an oxygen plasma.

General Considerations

A striking simulitude seems to exist between the self-sustaining dipole discharge in oxygen and electrolysis in an aqueous solution. The mechanism of oxidation by anodization is suspected to be similar in many ways in both systems. The difference is that one of them is in a liquid phase, the other in a gaseous phase. In fact, if the metal coated with oxide or other porous insulator is made the anode of an ionized oxygen cell, the self sustaining dipole discharge current sets up an electrostatic field in the insulating film or increases the field already present. Metal or oxygen ions may be pulled through the film causing continuous growth of oxide. The growth of anodic oxide film in the ionized gas cell is then a problem of ionic conduction at high field strength and transfer processes occur at two interfaces, metal - insulating film and insulating film - ionized oxygen.

It is obviously desirable to express the behavior of the growth in terms of some measure of the field strength in the insulating film. Contrary to the case of an electrolytic cell where difficulties due to the

electrochemical nature of the system occur, it is quite possible in the case of the self sustaining discharge to measure the field which exists between the electrode metal and the porous insulating film. For this, a suitable method would be to measure the electrostatic force which pushed the film into close contact with metal [by using, for example, a counter-balance weight] and hence to deduce the field value.

The film thickness can be controlled since the potential difference across the insulating film can be varied at will, whereas the tarnishing of metal in air is controlled by the thermodynamics of the system. At constant voltage, the growth of oxide thickens the insulating film at the surface of the electrode and causes a continuous decrease in the gradient of potential. Consequently, the ionic current decreases. The great fall of current observed in the self sustaining dipole discharge at constant voltage was probably due to this effect. It was due also to an unknown effect from the conducting gas since it was observed that if the gas was renewed during the experiment at constant applied voltage, the current returned almost to its initial value.

EXPERIMENTAL METHODS

Preparation of Films

Aluminum

A. Sodium-fluoride stripping layer

A rather thick layer of NaF was evaporated onto cleaned cover slips, and a layer of Al, approximately 1500 Å thick, was evaporated over the fluoride. The fluoride layer seemed to have rather a rough surface, probably because of the thickness, and several of the targets showed

a matte surface. The aluminum films were floated off on water, picked up on specimen screens, and electron micrographs were made.

B. Sodium-chloride stripping layer

A layer of NaCl, approximately 1000 Å thick, was evaporated on cover slips, and approximately 2250 Å of Al was evaporated over the NaCl. This surface seemed to be much more even than with the NaF stripping layer.

After reaction with the oxygen plasma, the films were floated off on water, but holes were left in the film in the most attacked places. Micrographs and selected area diffraction patterns showed sharp rings, which were identified as belonging to Al, and broad rings, as from amorphous material, with diameters giving spacings of approximately 2.2 Å and 1.2 Å.

The electron micrographs showed essentially the same picture as with NaF stripping layer.

C. Surface replicas

These were made by evaporating aluminum on cover slips without the stripping layer. After treatment in oxygen plasma, the surface was preshadowcast with Pt/Pd at an angle of approximately arctan 0.5, and the specimen covered with a 100-200 Å thick carbon layer while it was rotated to get a layer of uniform thickness. The carbon replicas were then floated off on 20% HF, washed in distilled water, and picked up on specimen screens.

Copper

Specimens were made by vacuum evaporation of copper on cover slips. Estimated thickness was 870 Å. After bombardment in oxygen plasma, the specimens were dry stripped, washed in acetone, and picked up on specimen grids.

Treatment in the Plasma

The following conditions obtained during exposure to the plasma discharge.

1. Metal films anodic.
2. Oxidation at constant discharge current of 0.2 mA/cm^2.
3. Oxidation time, 1 hour.
4. Distance between electrodes: 2 cm.
5. Voltage between electrodes, about 21 kV.
   Voltage adjusted to maintain constant current. This adjustment required variation of ± 0.5 kV.
6. Oxygen gas pressure 760 torr at 35°C. Slow flow of oxygen during experiment.

RESULTS

Figures 1 and 2 are transmission electron micrographs of aluminum films. Two stripping methods were used to see if these procedures introduced appreciable plastic deformations in the foils. The film in Figure 1 was prepared by evaporating aluminum onto a well cleaned glass surface. The film was then covered with collodion. After the plastic had dried, the metal together with the plastic could be stripped from the glass surface. The collodion was then dissolved in acetone. The film in Figure 2 was floated off from an evaporated NaCl base layer.

Both these micrographs show essentially the same fine grained structure of polycrystalline aluminum. Both structures seem free of any marked plastic deformations. The grain size is small, in the range from 100 to 500 Å.

The effect of exposure to the plasma discharge is shown in Figures 3 and 4. These films were prepared on sodium chloride layers.

Figure 3 shows the result of anodic oxidation of these films in the oxygen plasma. Amorphous material probably oxide and some aluminum are evident.

Figure 4 shows an area of moderately intense attack. The patchy distribution of the heavier oxide layers is noteworthy. It is typical of these oxidations to occur over regions about one micron in diameter, with other neighboring regions much less attacked.

Figures 5 and 6 show the results of quite heavy anodic attack on aluminum films over sodium fluoride. These films are more rough than those over sodium chloride.

Figure 5 shows a field from the edge of the attacked area; the film has been considerably torn up with holes having irregular edges. We can distinguish small regions of unattacked aluminum which contain dark loops of Bragg contrast. The lighter area shows more or less circular details 100 to 500 Å in diameter believed to be oxide. Figure 6 is a more heavily attacked area. Away from the holes some aluminum is still to be seen, but there is a great deal of oxide mixed with it. Electron diffraction powder diagrams of these specimens showed only aluminum. The oxide present was either too small in amount or too amorphous to be revealed.

The next pictures show the oxidation process by means of surface replicas. Figure 7 shows the virgin glass and Figure 8 is a replica of an unusually thick (about 1500 Å) aluminum film. The individual grains of aluminum which were seen on transmission (Figure 1) are apparently seen here also as surface structures in the replica. Figures 9 and 10 show an attacked area and a relatively unattacked area. Figure 9 probably corresponds in replica to the transmission picture of Figure 5. Figure 9 also shows

shows the beginning of crack formation. The upper right hand corner is region of mild attack, but one can see what may be tiny nuclei of oxide in the surface.

In order to secure further information about the oxide film a special procedure was tried. A thick aluminum film on glass was oxidized in the plasma and dry stripped with a collodion backing. The film was then left overnight in 1.5 N HCl to dissolve the aluminum, washed in water, dried, and the collodion dissolved in acetone. The very thin oxide films could then be taken up on the grid for examination in the electron microscope. The transmission picture is shown in Figure 11. The specimen is definitely crystalline, with small grains. This specimen had been left for 5 days in the laboratory at room temperature before stripping, and there may have been growth of grains during that time. Certainly the diffraction patterns were different from those of the amorphous oxides usually observed. The following lattice plane differences were found:

d	Rel. Intensity
1.96 Å	6
1.34	10
1.29	1
1.14	3
0.883	1
0.807	3

These spacings indicate an identification as δAl_2O_3 although not all the spacings listed on the A.S.T.M. card were found in the pattern. This absence may be due to differences in relative intensities between X-ray and electron diffraction and also to orientation effects. The first reported occurrence of δAl_2O_3 was in the product from heating $Al_2O_3.H_2O$ at 1000° in steam [H.C. Stumpf, A.S. Russell, J.W. Newsome, G.M. Tucker, Inc. Eng. Chem. 43 1398 (1950)]. It is rather strange

that it should occur as a product of oxidation of aluminum by plasma discharge. After its first detection in the specially prepared oxide films, we were able to find evidence for the δAl_2O_3 in several other oxidized samples.

Experiments on Copper Films

Only a few runs were made with evaporated copper film oxidized in the plasma discharge. The copper films were more coarse grained than the aluminum films, with extensive growth twinning in the crystallites. Selected area diffraction revealed Cu, Cu_2O and CuO. The Cu_2C lines were broad, tending to amorphous patterns, but the Cu lines were sharp and crystalline in nature. An electron micrograph is shown in Figure 1

CONCLUSIONS

The present study is obviously only a preliminary introduction to a field of great complexity. In the usual type of metal oxidation there is a reasonably well defined interface between the metal and the oxide, and the oxide grows at a single extensive interface between two phases. In the case of bombardment of metal by oxygen ions, the incoming ions would penetrate the surface of the metal to a depth of about 100 Å. We would then expect nucleation and growth of oxide below the outer surface of the metal. Some of the unusual morphology of the oxide layers in the experiments reported above may be a consequence of this multiple nucleation in depth of the oxide phase. Such nucleation and growth of oxide beneath the outer surface of metal was also reported recently by Meyer and Havmann [M. Meyer and P. Havmann, C.R. Acad. Sci. (Paris) 258, 6-0 (1964)].

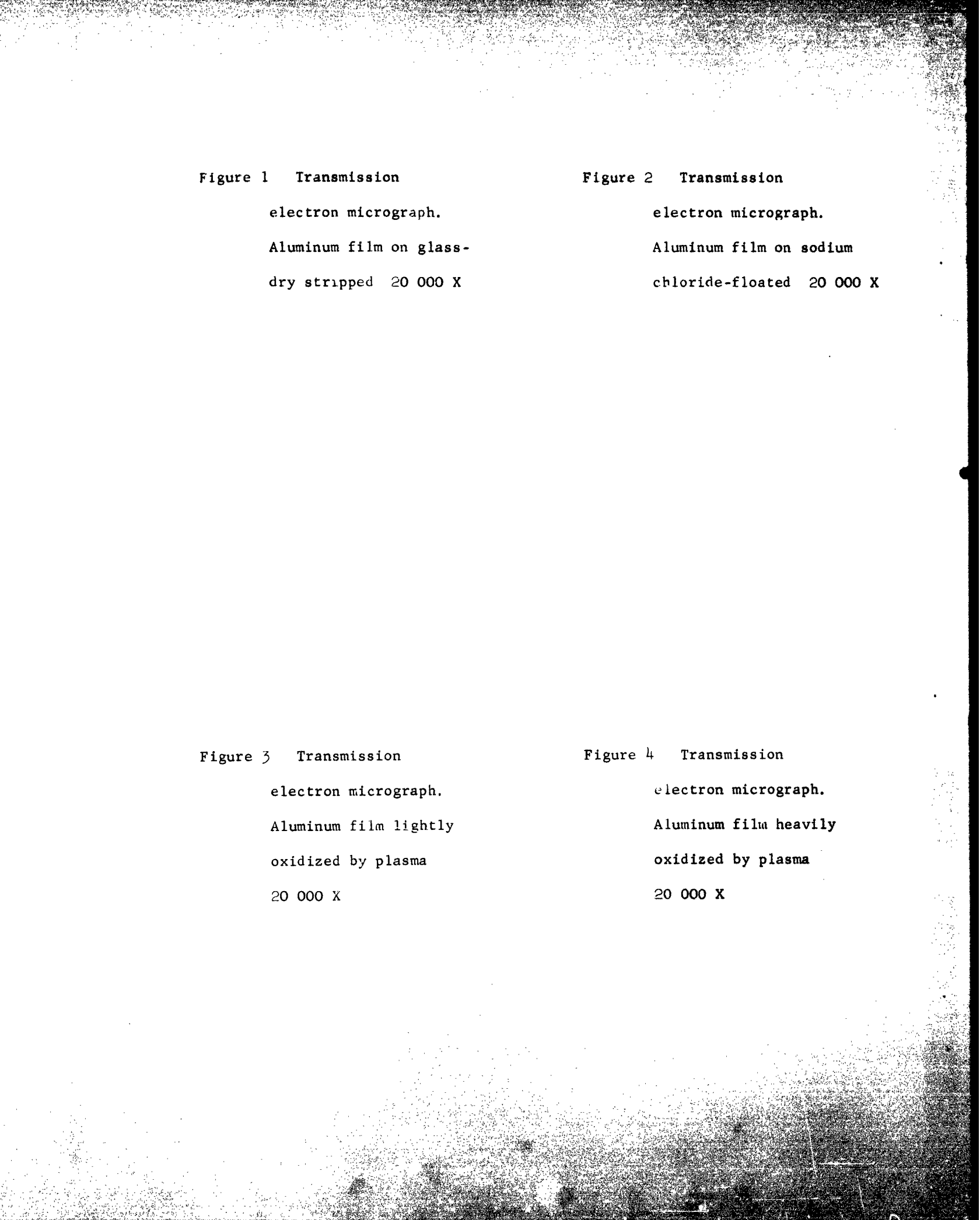

Figure 1 Transmission electron micrograph. Aluminum film on glass-dry stripped 20 000 X

Figure 2 Transmission electron micrograph. Aluminum film on sodium chloride-floated 20 000 X

Figure 3 Transmission electron micrograph. Aluminum film lightly oxidized by plasma 20 000 X

Figure 4 Transmission electron micrograph. Aluminum film heavily oxidized by plasma 20 000 X

Figure 5 Transmission electron micrograph of 1500 A aluminum film over sodium fluoride after anodic oxidation in oxygen plasma.

20 000 X

Figure 6 Similar to Figure 5 but more heavily attacked

20 000 X

Figure 11 Transmission electron micrograph of small grained aluminum oxide.

15 000 X

Figure 12 Transmission electron micrograph of 870 A copper film after anodic oxidation in oxygen plasma.

15 000 X

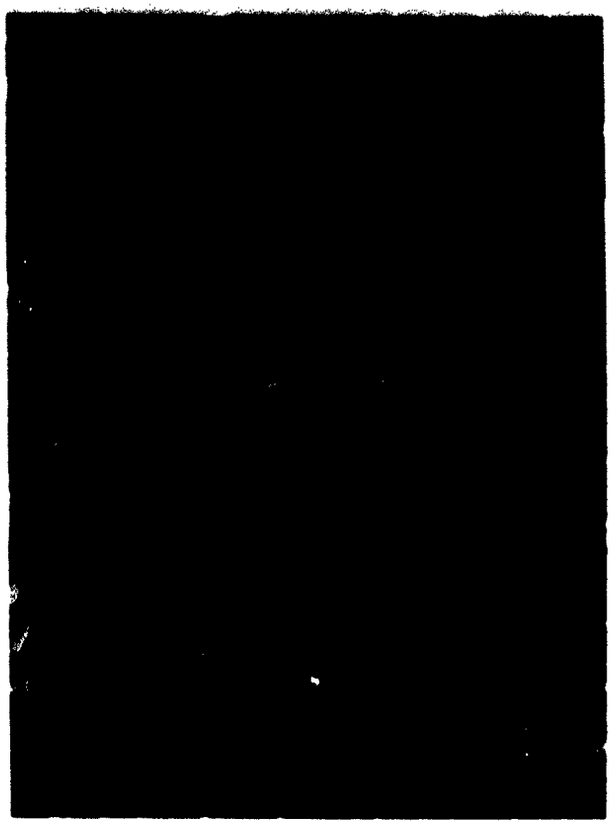

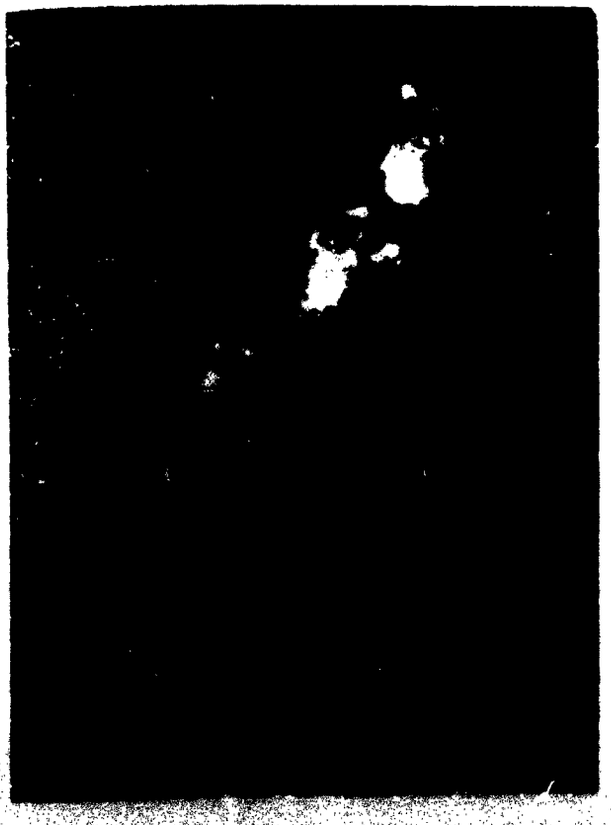

Figure 7 Pt/Pd Preshadowcast
Carbon Replica
15 000 X
Virgin Glass

Figure 8 Pt/Pd Preshadowcast
Carbon Replica
15 000 X
Evaporated Aluminum
film about 7500 A thick

Figure 9 Pt/Pd Preshadowcast
Carbon Replica
7500 X
Aluminum film heavily
attacked by oxygen
plasma.

Figure 10 As Figure 9
but more heavily
attacked.

OXIDATION OF ALUMINUM FILMS AFTER IONIC BOMBARDMENT WITH HELIUM OR XENON

Walter J. Moore, Sigemaro Nagakura, and Sylvester Brown

Chemical Laboratory, Indiana University
Bloomington, Indiana

ABSTRACT

Chemisorption of oxygen at 25°C has been measured on aluminum films prepared by evaporation in a high vacuum system (10^{-8} to 10^{-9} torr). The films were in some cases impregnated with helium or xenon by cathodic bombardment in a plasma or glow discharge. Occluded inert gases that could not be pumped off at 25°C were rapidly released on exposure of the treated film to oxygen. The results suggest that the initial attack of oxygen involves an immediate rearrangement of the aluminum atoms in the surface layers.

OXIDATION OF ALUMINUM FILMS AFTER IONIC BOMBARDMENT WITH HELIUM OR XENON

Walter J. Moore, Sigemaro Nagakura, and Sylvester Brown

Chemical Laboratory, Indiana University
Bloomington, Indiana

Our interest in this subject was aroused by some unusual observations on the behavior of polished aluminum targets bombarded with helium ions at 3 to 10 kv in an ionic beam apparatus. The effect of the bombardment was to protect completely the aluminum surface against corrosion in moist air in the presence of mercury vapor, an atmosphere that produced catastrophic corrosion of an unbombarded specimen. We suggested two possible explanations for this result: (a) It might be due to the deposition on the crystal surface of a tenacious layer of polymeric material, caused by decomposition of ambient or adsorbed gases by the ionic beams as it strikes the metal surface. (b) It might be due to some influence of the occluded helium on the reactivity of the metal toward oxygen and other corrosive gases.

In order to distinguish between these hypothetical mechanisms, we decided to try to repeat the experiment in an ultrahigh vacuum system (10^{-9} torr) free of oil vapors or other organic contaminants. The experimental difficulties of constructing an ionic-beam apparatus operating under such conditions led to a decision to use a more simple arrangement, in which the inert gases would be introduced by making the metal surface the cathode in a plasma or glow discharge.

EXPERIMENTAL PROCEDURES

The general features of the experimental system are shown in Figure 1. The system was constructed of welded stainless steel and Pyrex glass, except for Kovar metal to glass seals which were formed with Nicobraz LM solder to the stainless steel sections. The system was pumped during bake-out at 400-450°C with a 50 l/s mercury diffusion pump and the final pumping was with an Ultex 10-250 ion pump. A Consolidated Electrodynamics 21-612 residual gas analyzer was incorporated into the high vacuum side of the system.

Details of the reaction vessel are shown in Figure 2. It was constructed from a 2-liter Pyrex flask, with provision for evaporation of a metal coating onto the inside of the flask, and electrodes for striking and maintaining a discharge.

A calibrated storage volume and a dosing system allowed one to admit successive measured "shots" of oxygen or other gases to the system. Lower pressures were measured on Vactec ionization gauges with oxide coated iridium-ribbon filaments and higher pressures on Pirani gauges.

The inside of the bulb was coated with aluminum by evaporation from an electrically heated tungsten coil. The aluminum was first melted and outgassed before final evaporation. The mass of aluminum evaporated was from 15 to 40 mg, corresponding to a coherent film thickness of 690 to 1160 A. It is likely that aluminum evaporated under these conditions has a rough surface and somewhat porous structure. After evaporation of the aluminum, the system was again pumped to $\sim 10^{-8}$ torr prior to loading the film with inert gas. Figure 3 is an electron

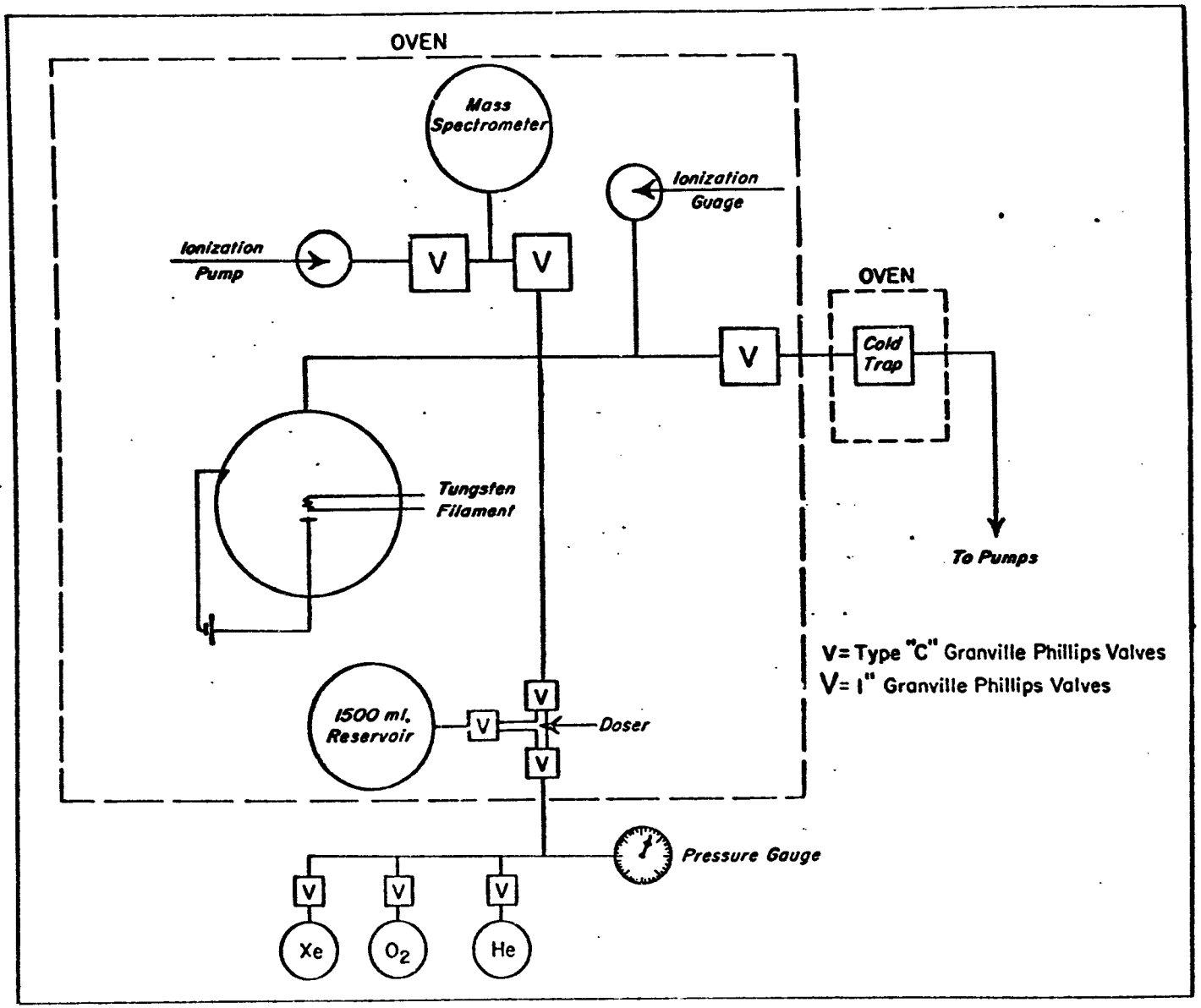

FIGURE 1

Schematic outline of apparatus.

FIGURE 2
The reaction bulb.

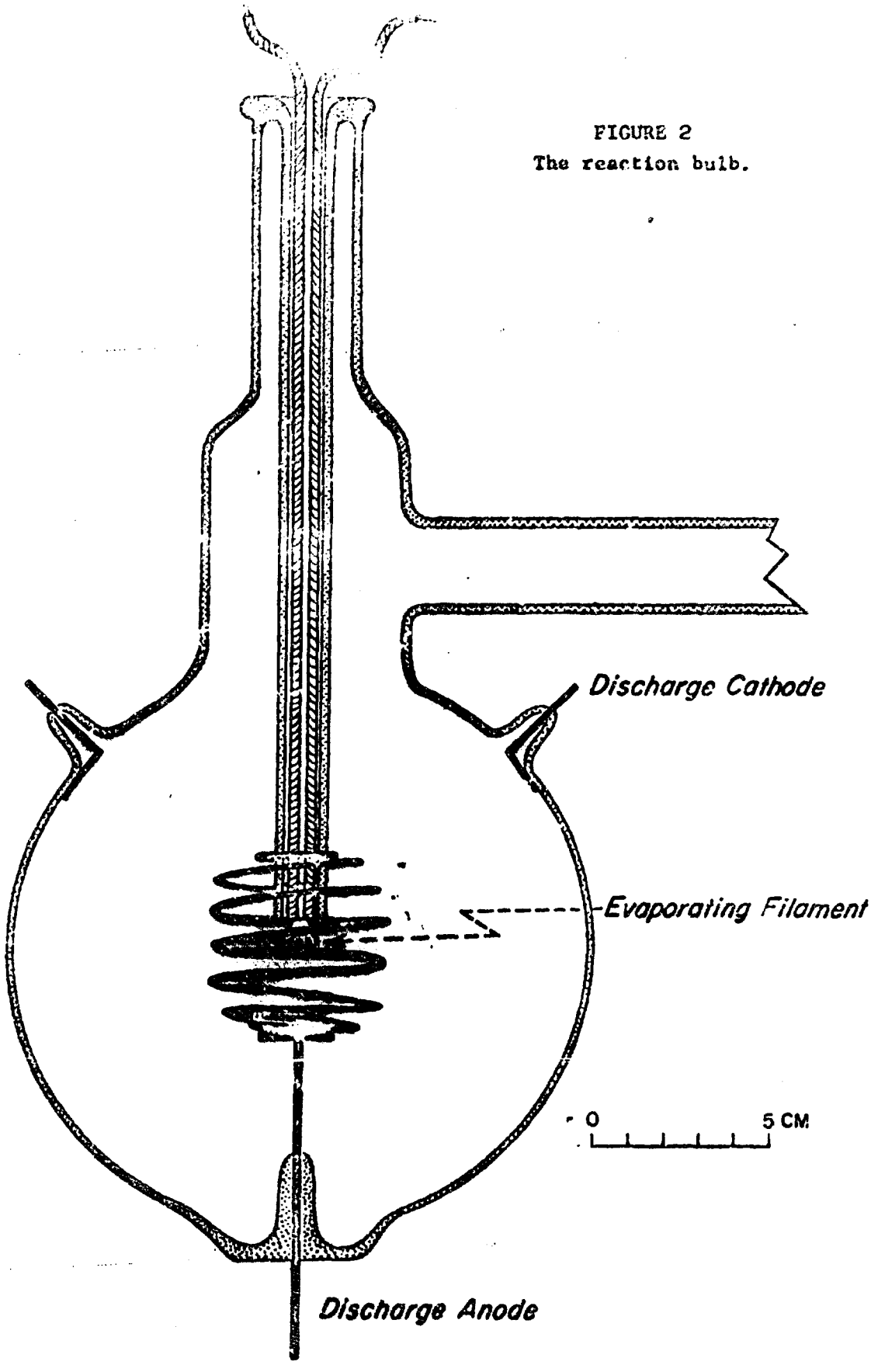

Figure 3. Electron micrograph of aluminum film after helium bombardment. Platinum shadowed.

80 00 ×

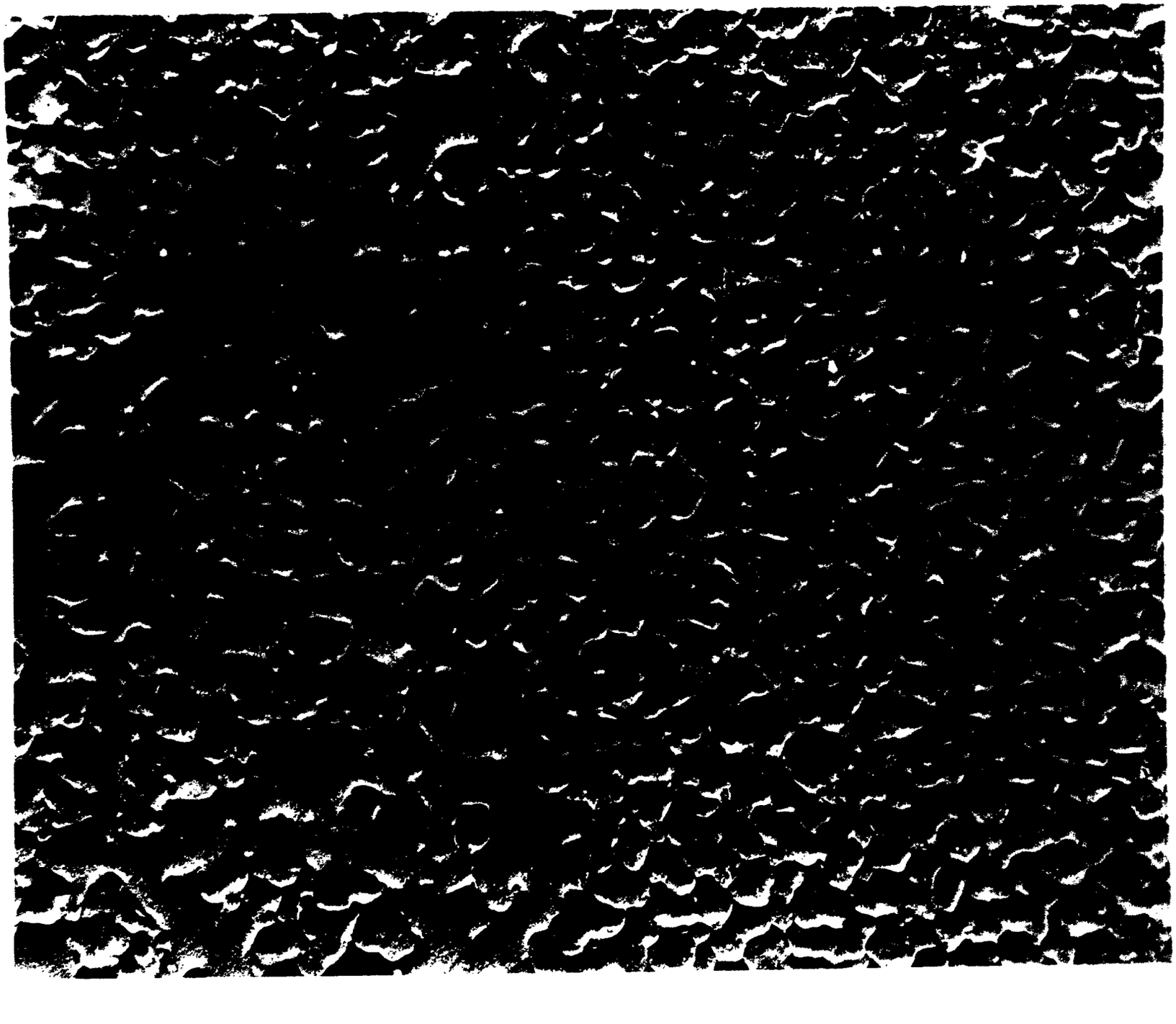

micrograph of an aluminum film after exposure to a helium discharge. We would expect the untreated film to look much the same.

In a typical bombardment with xenon the gas pressure was 10 to 20 micra. The voltage drop across the bulb was 300 V, and a current of 10 ma was drawn for 3 hours. It is evident that only a small fraction, of the order of 0.01, of the xenon ions incident on the aluminum film cathode became trapped beneath the film.

After bombardment with inert gas the bulb was pumped down to the 10^{-6} to 10^{-7} torr range, and the rate of evolution of gas measured before beginning the oxygen adsorption run. Some of the trapped inert gas was pumped away at this stage, but most of it remained trapped in the film

Oxygen adsorption and oxidation was followed by admission of successive small "shots" of oxygen from the doser. At regular time intervals the total pressure in the bulb was measured and the residual gas composition was measured with the mass spectrometer residual gas analyzer. The analyzer was not, however, continuously connected with the bulb during the oxidation run.

EXPERIMENTAL RESULTS

If a baked out, evacuated glass bulb is exposed to oxygen, there will be considerable adsorption of oxygen on the wall. In our system this amounted to about 70 ccmm. We do not know how much of this represents adsorption on the bare glass surface and how much on the metal tubing. [A blank adsorption run on the tubing alone must be made to secure these data].

The course of oxygen adsorption on an evaporated aluminum film is shown in Figure 4. It will be noted that the rate of oxygen adsorption decreases markedly after the first two shots. Each "shot" corresponds to an amount of oxygen equivalent to about a 5 Angstrom layer of Al_2O_3 based on the geometric surface area of the film. Based on the chemisorption of O atoms on closest packed planes of aluminum atoms, each shot corresponds to about one-third monolayer. As Figure 4 indicates, residual gas began to build up after 2 or 3 shots of oxygen, which would be consistent with attainment of a chemisorbed monolayer or about 10 A of Al_2O_3. When allowance is made for background adsorption, the total oxygen uptake at the end of 17 shots, when the residual pressure has reached 1.5×10^{-2} torr, is about 20 A on the basis of the geometric film area. This is less than we expected from published data.

Several runs were made with bombardment by helium ions prior to chemisorption of oxygen. In a typical run, the bombardment condition was 2 mA at 145 V for 10 hr. Under these conditions only about 1.5×10^{15} atoms He/cm^2 were taken up by the film, about one atom He for every eight Al atoms in the apparent surface. The effect of such a treatment with helium on the subsequent rate of uptake of oxygen was not great. It appeared, however, that some additional release of helium occurred when the oxygen struck the film. Since a greater amount of helium in the film led to a higher final pressure for a given amount of oxygen adsorption, some evidence for protection of the metal by occluded helium may be adduced.

The next step was to try to secure a higher incorporation of occluded helium by increasing the potential gradient across the discharge tube.

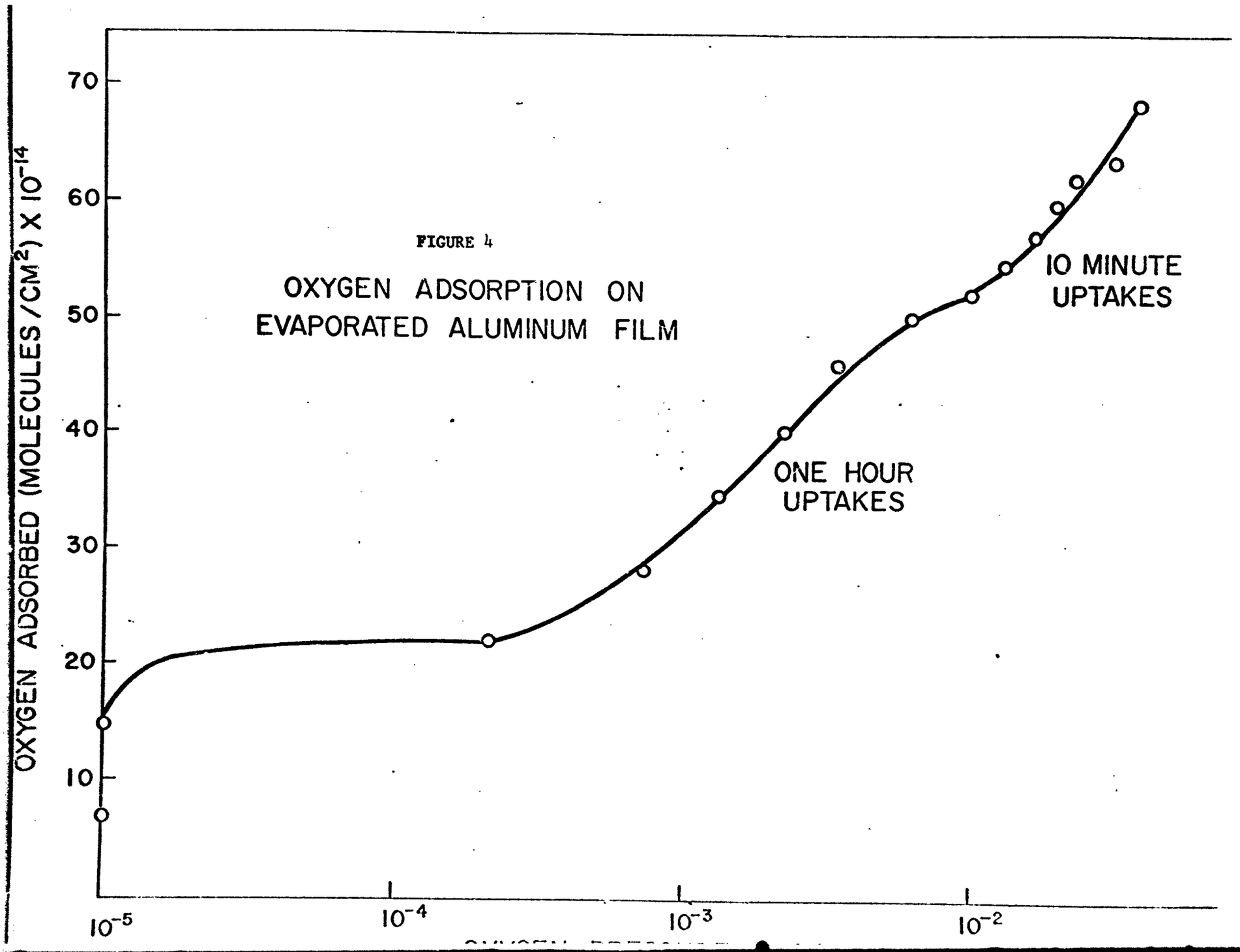
OXYGEN ADSORBED (MOLECULES/CM²) X 10⁻¹⁴
70
60
50
40
30
20
10
10⁻⁵
10⁻⁴
10⁻³
10⁻²
OXYGEN ADSORPTION ON
EVAPORATED ALUMINUM FILM
ONE HOUR
UPTAKES
10 MINUTE
UPTAKES

FIGURE 4

The helium pressure was lowered to 30μ and a discharge maintained at 1000 V for 2.15 milliampere hours. This gave an estimated $2.5 \times 10^{15}/cm^2$ helium atoms embedded. In this case also, no protective action was achieved, but there was direct evidence of helium evolution, as shown by the pressure-time curves of oxygen chemisorption, with and without prior helium bombardment. Subsequent studies were done with xenon as the impregnating gas and a mass spectrometer residual gas analyzer to monitor the composition during an adsorption run.

Mechanism of Helium Release

There are several mechanisms for the helium release upon oxygen chemisorption which may operate exclusively or in combination.

(a) The adsorbed oxygen may effectively replace helium atoms from the sites in which it is occluded.

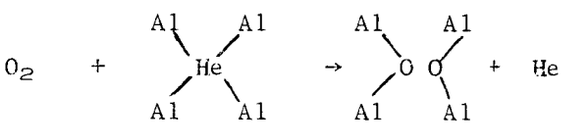

(b) The adsorption of oxygen may cause a displacement of the surface aluminum atoms sufficient to permit the escape of helium atoms. It would be difficult to distinguish this mechanism from (a).

(c) The release of heat when oxygen is chemisorbed on aluminum may raise the temperature in the surface layers sufficiently to permit the escape of helium by diffusion. Although we do not have these data for helium, similar experiments with xenon showed that the xenon release was approximately equivalent to the oxygen chemisorbed. This result would argue against any purely thermal effect. Each shot of oxygen is a small fraction of a monolayer so that the heat released per unit area of film may not be sufficient to cause an appreciable rise in local temperatures.

Effects of Xenon Bombardment

The xenon work was facilitated by the use of a residual gas analyzer which permitted us to analyze the composition of the gas after oxygen chemisorption. The mass range of the analyzer extended only to M/Q = 80 and hence did not include Xe^{+} at 129 to 136. However, a strong broad peak due to Xe^{+3} was obtainable at about M/Q = 43.5 arising mainly from ^{129}Xe, ^{131}Xe, and ^{132}Xe the most abundant xenon isotopes. The experiments on oxygen chemisorption subsequent to xenon treatment are summarized in Table 1. It will be noted that xenon is desorbed as oxygen is adsorbed. The interpretation of these results is similar to that of the helium experiments.

In conclusion we can state that the extreme passivity of aluminum surfaces originally observed after bombardment with He^{+} in an ion-beam apparatus has not been found in the case of pure aluminum films prepared under ultrahigh vacuum conditions and then impregnated with He or Xe from a glow discharge. It is likely, therefore, that the passivity found previously was due to the deposition of a thin tenacious layer of undetermined polymer on the metal surfaces. On the other hand, we have found evidence that the chemisorption of oxygen on aluminum films impregnated with inert gas is quite different from that on bare aluminum. Apparently chemisorption of oxygen displaces occluded helium or xenon in the films.

TABLE I

OXYGEN CHEMISORPTION ON
ALUMINUM FILMS AFTER
XENON BOMBARDMENT

RUN NO.	MASS Al-mg	XENON VOLTS	TREATMENT MA	TREATMENT HR	OXYGEN UPTAKE FINAL PRESSURE	OXYGEN UPTAKE CCMM OXYGEN ADSORBED	RESIDUAL GAS
1	17.5	300	10	3	4×10^{-3}	360	17% Xe
2	23	250	9	2	4×10^{-3}	300	---
3	41	2.5	30	3	$\sim 10^{-2}$	150	$\sim$ 30% Xe
4	42	500	9	1.5	$\sim 10^{-2}$	360	$\sim$ 50% Xe

UNCLASSIFIED

AD

Indiana University Chemical Laboratory, Bloomington, Indiana
APPLICATIONS OF IONIC BEAMS TO STUDY OF CORROSION OF METALS BY GASES, by Walter J. Moore. Technical Report, 40 p, figures, tables. (Contract DA-33-008-ORD-1989), DA Project 2001050[illegible]00, ACMS Code 5011.1002, ARCD Report 2698:1
Unclassified.

1. Corrosion
2. Metals-Gaseous Corrosion
3. Ionic Beams
4. Oxide Films

This final report is given in the form of a collection of preprints based on various sections of the work. The preprints are: (1) Effects of Atomic Oxygen on Semiconductor Oxides, by Nguyen Trinh Dzoanh and Walter J. Moore; (2) A Self Sustaining Dipole Discharge in Oxygen, by Nguyen Trinh Dzoanh; (3) Corrosion of Metal Films in an Oxygen Plasma at High Pressure; (4) Oxidation of Aluminum Films After Ionic Bombardment With Helium or Xenon, by Walter J. Moore, Sigemaro Nagakura and Sylvester Brown.

ADDITIONAL COPIES MAY BE OBTAINED FROM ASTIA. AD

UNCLASSIFIED

AD

Indiana University Chemical Laboratory, Bloomington, Indiana
APPLICATIONS OF IONIC BEAMS TO STUDY OF CORROSION OF METALS BY GASES, by Walter J. Moore. Technical Report, 40 p, figures, tables. (Contract DA-33-008-ORD-1989), DA Project 2001050[illegible]00, ACMS Code 5011.1002, ARCD Report 2698:1
Unclassified.

1. Corrosion
2. Metals-Gaseous Corrosion
3. Ionic Beams
4. Oxide Films

This final report is given in the form of a collection of preprints based on various sections of the work. The preprints are: (1) Effects of Atomic Oxygen on Semiconductor Oxides, by Nguyen Trinh Dzoanh and Walter J. Moore; (2) A Self Sustaining Dipole Discharge in Oxygen, by Nguyen Trinh Dzoanh; (3) Corrosion of Metal Films in an Oxygen Plasma at High Pressure; (4) Oxidation of Aluminum Films After Ionic Bombardment With Helium or Xenon, by Walter J. Moore, Sigemaro Nagakura and Sylvester Brown.

ADDITIONAL COPIES MAY BE OBTAINED FROM ASTIA. AD

UNCLASSIFIED

AD

Indiana University Chemical Laboratory, Bloomington, Indiana
APPLICATIONS OF IONIC BEAMS TO STUDY OF CORROSION OF METALS BY GASES, by Walter J. Moore. Technical Report, 40 p, figures, tables. (Contract DA-33-008-ORD-1989), DA Project 2001050[illegible]00, ACMS Code 5011.1002, ARCD Report 2698:1
Unclassified.

1. Corrosion
2. Metals-Gaseous Corrosion
3. Ionic Beams
4. Oxide Films

This final report is given in the form of a collection of preprints based on various sections of the work. The preprints are: (1) Effects of Atomic Oxygen on Semiconductor Oxides, by Nguyen Trinh Dzoanh and Walter J. Moore; (2) A Self Sustaining Dipole Discharge in Oxygen, by Nguyen Trinh Dzoanh; (3) Corrosion of Metal Films in an Oxygen Plasma at High Pressure, by Jens Trattetberg, Nguyen Trinh Dzoanh and Walter J. Moore; (4) Oxidation of Aluminum Films After Ionic Bombardment With Helium or Xenon, by Walter J. Moore, Sigemaro Nagakura and Sylvester Brown.

ADDITIONAL COPIES MAY BE OBTAINED FROM ASTIA. AD

Abstract cards are for use of recipient and may be removed.

Abstract cards are for use of recipient and may be removed.